TECHNISCHE UNIVERSITÄT WIEN
Vienna | Austria

ICEBE
IMAGINEERING NATURE

Diplomarbeit

Zeta-Potenzialanalyse von regenerierten Zellulosefasern

ausgeführt zum Zwecke der Erlangung des akademischen Grades einer Diplom-Ingenieurin (Dipl.-Ing. oder DI), eingereicht an der TU Wien, Fakultät für Technische Chemie, von

Rebecca JANKNECHT

Mat.Nr.: 01127798

unter der Leitung von

Senior Scientist Dipl.-Ing. Dr.techn. Andreas BARTL

Institut für Verfahrenstechnik, Umwelttechnik und technische Biowissenschaften, E166

Wien, Juli 2020

Stadt und Datum *Unterschrift*

Acknowledgements

I would like to express my sincerest gratitude to Lenzing AG (Austria) for offering me a master's thesis at their company. In particular, I would like to thank my two incredible supervisors Dr. Martina Opietnik and Dr. Axel Rußler, who have placed their great trust in me from the very beginning and have always supported me with their most valuable advice and experience in the field of research. You have not only guided me through the master thesis but also through the last months of my life and I am grateful for your encouragement and the sympathy you have shown me. Appreciation is also extended to the members of the research department for their support, with special thanks to my laboratory colleague Markus Hager, for the interesting discussions about science and life and for the many moments when we laughed together over coffee and cake.

I would like to especially thank my thesis advisor Dr. Andreas Bartl, for his guidance and his constant support during the last six months. I thank him for his kindness and helpful suggestions during the process of this thesis, even though it took a second attempt.

I would like to express my very great appreciation to Dr. Thomas Luxbacher from Anton Paar for his valuable and constructive suggestions during the development of this research work. His many years of experience in the field of zeta potential analysis were a great help in evaluating the results and his willingness to make his time available so generously has been very much appreciated.

My gratefulness is also extended to Prof. Peter Weinberger, who taught me that courage is always the right choice, and Prof. Paul Mayrhofer, who has thankfully offered his time as third examiner and supported me during the administrative process.

Finally, I express my very profound gratitude to my parents, my fiancée Markus and all my dear friends Vanessa, Jessica, Ezgi, Ebru and Frieda for providing me with unfailing support and continuous encouragement throughout my years of study and through the process of researching and writing this thesis. This accomplishment would not have been possible without them.

Thank you.

"The discipline of the writer is to learn to be still and listen to what his subject has to tell him."

Rachel Carson (1907–1964)

Table of Contents

English Abstract

In the presented master thesis, the zeta potential of different types or regenerated cellulose fibers has been investigated in order to compare the differences in the electrochemical properties of various Lyocell and viscose fibers from Lenzing AG (Austria). In view of the fact that the zeta potential analysis of regenerated cellulose fibers is restricted to apparent values due to bulk material swelling and the complex structure of the fiber surface, further background information on chemistry and surface charge of cellulose fibers were prepared in this thesis. In addition, the manufacturing process significantly influences the different structural and morphological properties of both Lyocell and viscose fibers. The theory of zeta potential analysis of macroscopic solids focusing on cellulosic fibers, and the description of the electrokinetic analyzer used are of further interest. The results represent individual electrokinetic properties of both treated and untreated Lyocell and viscose fibers, indicating differences in their inherent surface structure and/or different physiochemical properties. In search for a fast and reliable method for surface charge analysis of various Lyocell and viscose fibers, the application of the streaming potential technique proved to be a suitable measuring method, although there are limitations concerning the complex behavior in aqueous solutions.

Deutsche Kurzfassung

In der vorliegenden Diplomarbeit wird die Bestimmung des Zeta-Potentials von unterschiedlich modifizierten cellulosischen Regeneratfasern der Firma Lenzing AG (Österreich) durch die Anwendung von Strömungspotentialmessungen beschrieben. Hierzu wird ein Überblick über den Aufbau und die physiochemischen Eigenschaften der Cellulose, die Unterschiede im Herstellungsprozess sowie die daraus folgenden strukturellen Eigenschaften der beiden wichtigsten cellulosischen Regeneratfasern Lyocell und Viskose gegeben. Eine Beschreibung des Messaufbaus sowie die theoretischen Aspekte der Zeta-Potential Analyse von makroskopischen Feststoffen setzen weitere inhaltliche Schwerpunkte. Die Darstellung der Messergebnisse in Abhängigkeit vom pH-Wert und der Ionenstärke der Elektrolytlösung repräsentieren die unterschiedlichen elektrokinetischen Eigenschaften von Lyocell- und Viskosefasern, bedingt durch die Unterschiede in ihrer supramolekularen und morphologischen Struktur. Ferner zeichnet sich der erzielte Effekt der entsprechenden Faserbehandlungen deutlich sichtbar in den elektrokinetischen Messungen ab. Unter Berücksichtigung des komplexen Verhaltens von cellulosischen Regeneratfasern in wässriger Lösung und den daraus folgenden Einschränkungen in der Bewertung der generierten Zeta-Potential Werte erweist sich die Anwendung des Strömungspotentialprinzips als rasche und reproduzierbare Messmethodik.

List of Figures

List of Tables

List of Abbreviations and Symbols

ASTM I	American Standard for Testing and Materials I
Ag	Silver
AgCl	Silver chloride
AGU	Anhydroglucose unit
AKD	Alkyl ketene dimer
Al^{3+}	Aluminum cation (3+)
$AlCl_3$	Aluminium chloride
$Al(H_2O)_6Cl_3$	Aluminum chloride hexahydrate
Ca^{2+}	Calcium ion (2+)
$CaCl_2$	Calcium chloride
Cl^-	Chloride
CLY	Lyocell
CO_2	Carbon dioxide
CRU	Constitutional repeating unit
CS_2	Carbon disulfide
CV	Viscose
DP	Degree of polymerization
DS	Dried state
EDL	Electro(chemical) double layer
HCl	Hydrochloric acid
H_2O	Water
H_3O^+	Hydronium
H_2S	Hydrogen sulfide
HSO_3^-	Hydrogen sulfite
H_2SO_3	Sulfurous acid
ICP-MS	Inductively coupled plasma mass spectrometry
IEP	Isoelectric point
KA1	Cationic additive 1
KA2	Cationic additive 2
K^+	Potassium cation (1+)

KCl	Potassium chloride
LENZINGViscostar®	LENZINGViscostar® is a trademark of Lenzing AG
MCC	Microcrystalline cellulose
Mg^{2+}	Magnesium cation (2+)
$MgCl_2$	Magnesium chloride
NaOH	Sodium hydroxide, soda lye
Na_2S	Sodium sulfide
NBAA	Never dried after avivage
NDBA	Never dried before avivage
NMMO	*N*-methylmorpholine *N*-oxide
NW	Nonwoven
OH^-	Hydroxide
p. a.	pro analysi
PI	Permeability index
pH	Power of hydrogen
K_a	Acid dissociation constant
REFIBRA™	REFIBRA™ is a trademark of Lenzing AG
SS1	Stock solution 1
SS2	Stock solution 2
SS3	Stock solution 3
S4	Solution 4
S5	Solution 5
SO_2	Sulfur dioxide
TENCEL™	TENCEL™ is a trademark of Lenzing AG
VisCBC	Viscose Continuous Batch Cooking
WA	Without avivage

ε_0	Permittivity of free space
ε_r	Relative permittivity
ζ	Zeta potential, electrokinetic potential
ζ^*	Zeta potential in swollen state
η	Dynamic viscosity
κ	Electrolyte conductivity
κ_{high}	Electrolyte conductivity at high ionic strength

κ^{-1}	Debye length
π	Pi (mathematical constant)
ρ	Material density
Ψ	Surface potential
°C	Degree Celsius
A	Sample area
d	Distance
d_f	Fiber diameter
e	Elementary charge
g	Gram
I	Ionic strength
dI_{str}	Streaming current
ΔI_{str}	Streaming current
k_B	Boltzmann constant
l	Liter
L	Sample length
$\frac{L}{A}$	Cell constant
L_f	Fiber length
m	Meter
mm	Millimeter
µm	Micrometer
mol	Mole
N_A	Avogadro number
Δp	Pressure ramp
R	Electrical cell resistance
R_{high}	Electrical cell resistance at high ionic strength
s	Second
S	Normalizing factor
mS	Millisiemens
T	Absolute temperature
T_t	Titer, linear density
dU_{str}	Streaming potential

ΔU_{str}	Streaming potential
V	Voltage
mV	Millivolt
w	Fiber weight

I Introduction and Motivation

It is well established that the surface charge of regenerated cellulose fibers is an essential feature of their physiochemical properties, which strongly affects the post-treatment and the final properties of cellulose fiber-based products, like textiles or nonwoven materials [1–3]. The surface charge correlates with the number of functional groups and varies with the origin and chemical processing of the cellulose material. It significantly influences the bonding strength of the fiber network and the adsorption properties of cellulose with respect to hydrophilicity and swelling, or to chemical components, e.g., surfactants, dyes, polyelectrolytes or metal ions.

The main functional groups present in cellulose fibers are carboxyl and hydroxyl groups and dissociate when brought in contact with a neutral or alkaline aqueous solution, remaining a negative charge. It is obvious that a better understanding of the nature of surface charge is essential for a specific modification of the physiochemical properties of regenerated cellulose fibers with regard to product and process development [1–4].

Some studies reported the determination of surface and/or total charge of natural and regenerated cellulose fibers by different titration methods, including conductometric and potentiometric titration as well as polyelectrolyte adsorption [1,5–9]. The integration of these analytical methods into the research operations proves to be cumbersome and time-consuming in many respects and contradict the demand for a fast and reliable analytical method with a high degree of automation. Ensuring a stable dispersion without grinding the fibers into small particles contributes an additional challenge for the feasibility of the titration methods mentioned. It is known from previous experiments that even staple fibers tend to wrap themselves around the stirrer, thus impeding a continuous and reliable performance of the analysis. The experimental approach to achieve a homogeneous dispersion by the application of ultrasound turned out to be successful, but difficult to implement.

In comparison, the streaming potential or streaming current analysis proves to be a more applicable method for comparative investigations of surface charge analysis of different cellulosic materials, especially viscose and Lyocell fibers [10,11]. The streaming potential or streaming current measurement of macroscopic surfaces is a powerful characterization tool in recent research and can be applied to various scientific fields, such as membrane and filter science, biomaterials, semiconductor devices, polymer surface characterization, or natural

and man-made fibers [11,12]. With regard to the experimental technique used, the information about the surface charge is expressed as the zeta potential ζ.

The streaming potential and streaming current method are implemented in the used electrokinetic analyzer SurPASS™ 3 by Anton Paar, which features a fully automated zeta potential analysis of macroscopic solids in real-life conditions. Not only the characterization of surface properties of various materials but also the adsorption and interaction processes of different components at the solid-liquid interface can be investigated [13].

In order to meet the increasing demand on multifunctional and biodegradable textiles and nonwoven materials, the knowledge regarding the surface charge of regenerated cellulose fibers in combination with suitable analysis methods is of essential importance. However, the interpretation of zeta potential surface analysis of regenerated cellulosic fibers may be difficult due to bulk material swelling and the complex structure of the fiber surface. Based on these considerations further background information on chemistry and surface charge of cellulose fibers were prepared in this thesis. In addition, the manufacturing process significantly influences the different chemical and structural properties of both viscose and Lyocell fibers.

II Cellulose and Wood

The main constituents of all wood species can be represented by cellulose, hemicelluloses and lignin. Cellulose as the most common and major biopolymer is of great importance as raw material. By far, the predominant use of industrially produced cellulosic fiber material are paper and textiles. Besides commercially important sources such as wood and cotton, other natural sources to be mentioned are algae, (e.g., *Valonia ventricosa, Chaetamorpha melagonicum)* [14] and cellulose of animal origin [15], but rather exceptional. Furthermore, acetic acid-producing bacteria such as *Gluconacetobacter xylinum* and *Acanthamoeba castellani* are able to produce pure cellulose from organic carbon sources [16,17].

II.I Structure of Cellulose

Cellulose is a homopolysaccharide consisting of long unbranched linear chains of linked anhydroglucose units (AGU). The AGUs are connected by ß-1,4-glycosidic linkages resulting in a rigid and straight conformation with neighboring monomer units being rotated by 180° with respect to each other. Thus, the constitutional repeating unit (CRU)) of cellulose is the *cellobiose* (4-O-β-D-Glucopyranosyl-β-D-glucopyranose), demonstrated in Fig. II.I.

The structural properties of the cellulose chain molecule result in different reducing effects at both ends: The terminal C-1 bearing hemiacetal functionality shows reducing activity, whereas the C-4 position is non-reducing. Therefore, each cellulose chain is terminated with a non-reducing and a reducing end as shown in Fig. II.I.

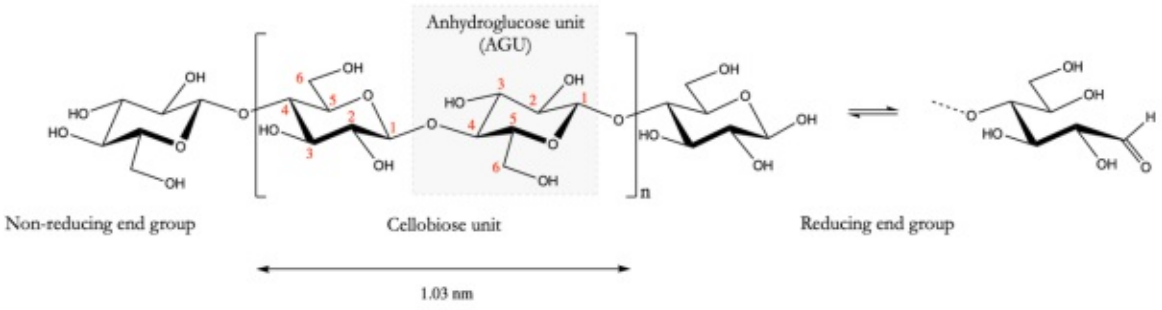

Fig. II.I Cellulose chain composed of cellobiose subunits with both reducing and non-reducing end group.

The reducing end groups are the only naturally occurring carbonyl functionalities in cellulose. They are highly likely to be present as hemiacetals, but only to a small extent as aldehydes and aldehyde hydrates [18–20].

II.I.I Polydisperse System

Cellulose as synthesized by nature is to be considered a polydisperse molecule. Since the number of anhydroglucose units in molecular chains vary from each other, not all cellulose macromolecules are of the same length in a native system. Therefore, the degree of polymerization (DP) of cellulose represents always an average value. It is assumed that native cellulose in wood has a very high degree of polymerization (up to 10'000 or more) [21,22], however, there are considerable variations depending on the source of cellulose and their pre-processing. Furthermore, any kind of chemical treatment tends to decrease the degree of polymerization. This chain-length shortening is mainly caused by isolations and purification procedures, (e.g., pulping and bleaching) since cellulose in higher plants is always incorporated into a matrix of hemicelluloses, lignin and low molecular-weight extractives [23]. This reduction in chain length (hydrolysis) is accompanied by the introduction of functional groups, such as carbonyl and carboxyl groups, or lactones. [19, 24]. Even environmental influences (natural aging) cause a number of autoxidative reaction to reduce DP values. For regenerated cellulose only a DP of approx. 250 to 800 is reported [22].

The mechanical properties of cellulosic fiber materials are related to the degree of polymerization of the constituent cellulose molecules and so to the chain length distribution. For instance, the DP is a determining factor when it comes to fiber strength. If the average molecular weight is decreasing below a certain number, it will cause significant deterioration in strength [15,21,23–25].

II.I.II Supramolecular Structure of Cellulose

Even if the molecular structure of cellulose seems rather simple, the inherent ability to organize itself in an extensive network of different types of hydrogen bonds makes it an extremely complicated material with complex supramolecular structure. The very stable ß-1,4-glycosidic linkages are reinforced by intramolecular hydrogen bonds formed between O-3(H) and O-5´of the adjacent AGU. A second intramolecular hydrogen bond between O-2(H) and O-6' is shown in Fig. II.II, providing an even more rigid configuration, however, its existence depends on certain arrangement criteria of the chains to each other. In addition,

adjacent cellulose chains are interconnected by various types of hydrogen bonds resulting in a supramolecular entity. These intermolecular linkages are responsible for the formation of highly ordered *crystalline* domains, (i.e., fibrillar units) and fundamental for the majority of properties of cellulose. Less-ordered *non-crystalline* region in the supramolecular structure are considered amorphous [20,26–33].

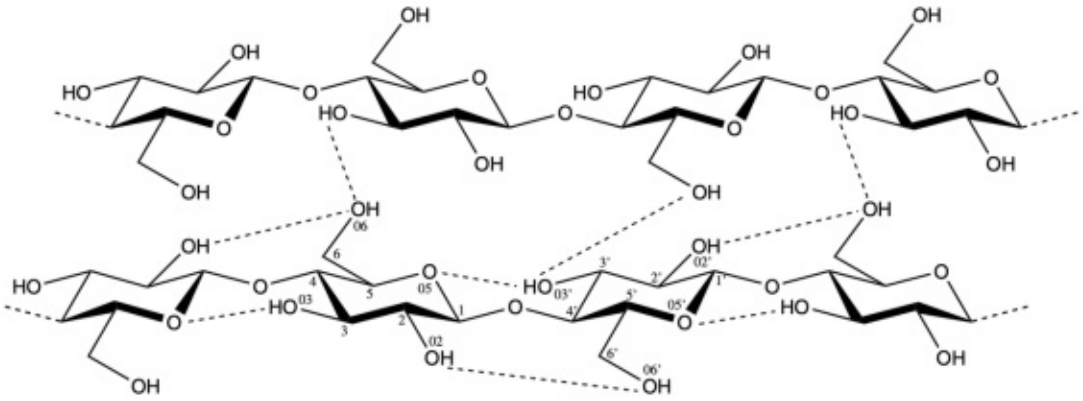

Fig. II.II Intra- and intermolecular hydrogen bonds in cellulose I according to Liang and Marchessault [31].

Cellulose considered as a polymorphic material can adopt different crystal structures. Native crystalline cellulose occurs as cellulose I and is composed of two coexisting phases known as I_α and I_β. Native cellulose can be converted into the thermodynamically more stable cellulose II modification by sufficient treatment with strong alkaline solutions or when it is precipitated from a dissolved state (e.g., Lyocell process). By comparison, the supramolecular aggregation of hydrogen bonds in cellulose II is more complex as it occurs in cellulose I, but is the most important form from a technical perspective. In cellulose II, the formation of intermolecular hydrogen bonds is favored and thus a higher packing density of the molecular chains and shorter average bond length. Other allomorphs (e.g., cellulose III_I, III_{II}, IV_I and IV_{II}) are obtained from cellulose I at elevated temperatures or by special chemical treatments and of minor importance only [20,34–36].

II.II Structural Characteristics of Wood

II.II.I Wood Components

Native cellulose has so far been described as linear but semicrystalline polymer consisting of highly structured crystalline regions (fibrils) as well as amorphous parts. But in nature, cellulose in its pure form is only present in limited extent. In almost pure form it is found in

the seedhair of cotton (*Gossypium sp.*) or kapok (*Ceiba pentanadra sp.*) [22]. However, wood or other lignocelluloses offer a far greater source of raw material for cellulose, but mostly combined with lignin, hemicelluloses, and other accessory compounds (extractives). The content of cellulose in wood varies according to origin and species between 30 – 50% [22]. Hemicelluloses or *polyoses* constitute 20 – 30% of wood [37]. Unlike cellulose mentioned as linear homopolysaccharide, hemicelluloses are branched polymers consisting of several sugar moieties, where xylose and glucose are often referred to as most abundant monomeric units [38]. Relative to cellulose, they have lower molecular masses with a DP lower than 200 and are removed during purification steps by alkaline extraction [39–43].

The amount of lignin present in wood species ranges from 20 – 40%, hence it is the third major polymeric component building up the wood cell walls [37]. The three-dimensional network of lignin consists of phenylpropane units linked by alkyl-alkyl, alkyl-aryl, and aryl-aryl groups (structure and characteristics of lignin) and its complex and irregular molecular structure cannot be expressed by a structural formula. Lignin is extracted from wood hydrolytically, or converted to a soluble derivative. Linkages have to be broken to free the cellulosic fibers during chemical pulping operations [43,44].

In addition, wood contains several thousands of other low- and high molecular compounds (wood extractives), which can be extracted with either neutral organic solvents or hot water. Terpenes, fats, waxes, sterols, phenolic compounds and inorganic salts have many different functions in wood and affect the properties to varying degrees, (e.g., swelling, biodegradability, stability, color, reserves of energy, protection, etc.) [30,32]. The chemical composition of wood varies according to origin and species. A rough distinction is usually made between *hardwood* and *softwood* [1] [46].

II.II.II Ultrastructure of Cell Walls and Morphology

The wood cell wall is composed of the three main structural components cellulose, hemicelluloses and lignin. While cellulose is characterized by a partially ordered semi-crystalline structure, hemicelluloses and lignin are amorphous. The framework structures consist of cellulose chains ordered in form of microfibrils formed by intermolecular hydrogen bonds, i.e., microfibrils are aggregates of elementary fibrils surrounded by shorter

[1] Botanically, woods are classified in *angiosperms* or conifers (softwoods), and *gymnosperms* or broad–leafed trees (hardwoods).

hemicellulose chains. The microfibrils form macrofibrils again, building up wall layers with different thickness and microfibril's orientation. Lignin and the hemicelluloses are incorporated between the cellulose microfibrils, which are chemically linked together. Thus, resulting in a close but irregular fiber cell wall architecture.

As illustrated in Fig. II.III, the cellulose fiber cell wall morphology is composed of several individual cell wall layers in a concentric arrangement, differing in their chemical composition and fibrillar orientation [46–49].

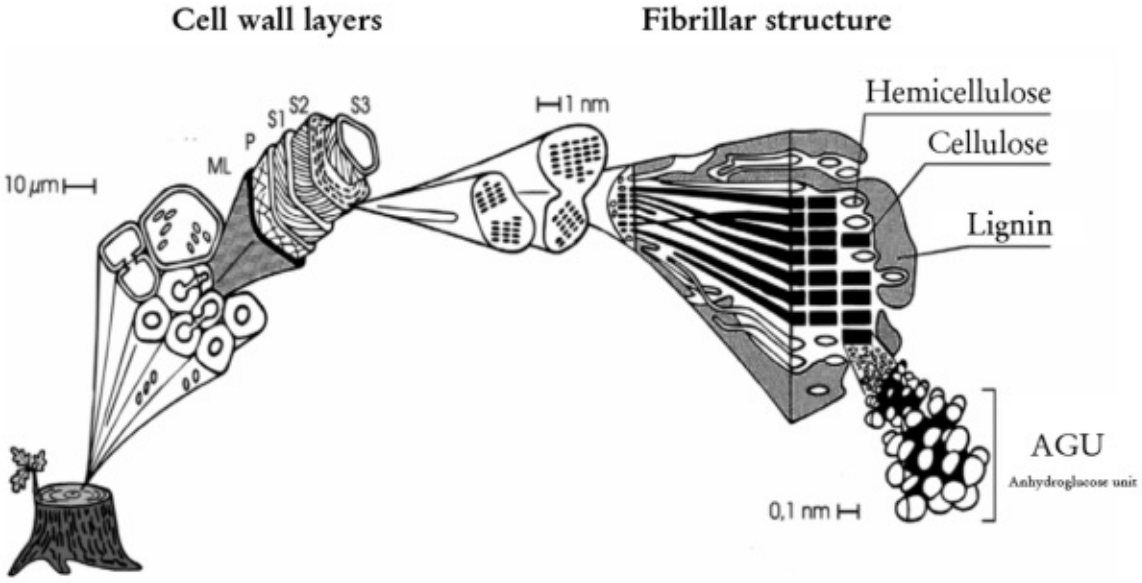

Fig. II.III Individual cell wall layers with fibrillary structure and their chemical composition, adopted from [50].

In addition to the fibrillar morphology, there is a system of pores, capillaries, voids, and interstices present in the fibrillar system. These perceptions in organization of structural components within the cell wall layers and arrangement of cellulose microfibrils proved to be determining for the characteristics of wood cell walls with regard to e.g., strength and density properties, dissolution mechanism, or swelling behavior [15,51].

III Chemical Pulping Processes

Cellulose as a plant origin offers an almost inexhaustible and sustainable source of raw material. Through pulping, wood or other lignocellulosic material is reduced to a fibrous mass, denoted as pulp. For industrial paper and fiber production, pulp is obtained from hardwoods and softwoods. This process of defibration within the wood structure is accomplished commercially by mechanical, chemical, or semi-chemical treatments. In chemical pulping, the fibers are separated through chemical reactions at elevated temperatures (130-170 °C) [52], but without further mechanical defibration. However, a sufficient degree of delignification is required. The characteristics of pulps obtained from different processes are decisive for further applications. Depending on the wood species and its chemical composition, the dissolution of wood components differs for each pulping process [53].

Since cellulose cannot be melted and is insoluble in the most common solvents, the processing into regenerated cellulose fibers shows more complexity compared to petroleum-based polymers [54]. With regard to the global environmental impact of industry, the recycling of valuable resources requires new technical approaches (e.g., Lyocell fibers with REFIBRA™ technology)[2] [55,56].

III.I Dissolving Pulp

Pulps are predominantly produced by chemical pulping processes, but only 2–3% of annual pulp production applies to high purity chemical pulp, i.e., dissolving pulp for regenerated fibers and cellulose derivatives [54]. The use of chemical pulps in Lyocell and viscose fiber production places much higher quality demands compared to pulps for the paper industry. Dissolving pulp is characterized by high cellulose content with a minimum amount of inorganic and non-cellulosic organic impurities. For the production of dissolving wood pulp, the prehydrolysis Kraft and the acid sulfite processes are used comprising additional purification stages [53]. Whereas the pulping process for papermaking pulps is intended to

[2] REFIBRA™ is a trademark of Lenzing AG

maintain the content of hemicelluloses, due to essential strength properties and cost savings, they have to be largely removed in oder to produce dissolving pulps.

In the viscose and Lyocell manufacturing process certain pulp properties are required to produce high-quality fibers, e.g., a high content of non-cellulosic impurities such as hemicelluloses or inorganic compounds affects the quality of the regenerated cellulose fibers and can lead to process issues [57–59]. The Lyocell process in particular comprises challenging demands on pulp quality since the pulp is dissolved directly in the solvent without the formation of an intermediate cellulose derivative [60–62]. In terms of processability of dissolving pulp, the reactivity towards derivatives or solvents is related to the accessibility of chemicals to the functional groups within the cellulose. Therefore, a reliable analytical characterization of dissolving pulps is essential for optimum process conditions and high product quality [63].

III.I.I Kraft Pulping Processes

Commercial Kraft or sulfate pulping accounts for 89% of the chemical pulps and dominates as the principal cooking process for paper pulps. By using NaOH and Na_2S as main active chemical agents, a selective delignifation process at high pH (12 to 13.8) [64] is accomplished. During the cooking process (140–175°C) [65], lignin is cleaved to short fragments that dissolve in the alkaline solution [66,67]. Initially, the α-aryl and β-aryl ether bonds in the phenolic units within the lignin structure react with hydroxide and hydrosulfite anions present in the aqueous cooking liquor. Further cleavage of β-aryl bonds in nonphenolic units continue the degradation until a certain limited degree of delignification is reached. The enriched cooking liquor containing a complex mixture of degraded lignin and carbohydrate substances is removed after countercurrent washing of the unbleached pulp. Since the Kraft process is not capable of removing the lignin completely, the Kraft pulp is subsequently bleached to eliminate the residual lignin and color [53,68].

Since hemicelluloses are comparatively resistant under alkaline conditions, conventional alkaline pulping processes are not suitable for the high-purity specifications of dissolving pulps. In order to prevent yield losses due to alkaline hydrolysis of cellulose under increased reaction conditions and precipitation of short-chain hemicellulose fractions, a prehydrolysis step is applied prior to the Kraft cooking process. This selective solubilization of hemicelluloses in wood is achieved by hydrolysis in water, mineral acids, or acetic acid [53,69–73]. Progresses in Kraft cooking over the past two decades led to the development

of Visbatch© and VisCBC (abbreviation for "Viscose Continuous Batch Cooking") process combining the advantages of displacement technology and steam prehydrolysis [74–77].

III.I.II Sulfite Chemical Pulping

Sulfite pulping covers the pulping process of wood with aqueous solutions of hydrogen sulfites (HSO_3^-) and sulfur dioxide, usually performed under acidic conditions [53,64]. Both hemicelluloses and lignin can be removed in the same process step. The procedure primarily is characterized by the type of base chemical used with sulfurous acid in order to effect delignification, and further by its acidic conditions. During (acid) sulfite cooking the equilibrium in terms of free SO_2 and combined sulfur dioxide (HSO_3^-) [Eq. (III.I)] needs to be balanced to assure sufficient delignification, but limited condensation reactions [53].

$$SO_2 + H_2O \rightleftharpoons H_2SO_3 \rightleftharpoons HSO_3^- + H^+ \qquad \text{(III.I)}$$

The cleavage of the glycosidic linkages (heterogenous hydrolysis) in hemicelluloses occurs randomly under acidic conditions and more rapidly than within the cellulose structure until the desired degree of cooking is achieved [78]. The predominance of sulfite pulping in dissolving pulp production is based on higher pulp yield, improved bleaching operations, and higher reactivity, compared to the prehydrolysis Kraft process. However, most softwoods and some hardwoods are considered less suitable for sulfite pulping [53]. For the production of their viscose fibers, Lenzing AG (Austria) gains dissolving pulp, inter alia, from beech wood by acid magnesium sulfite pulp processing [79].

III.II Bleaching

The (acid) sulfite process provides comparatively bright chemical pulps, whereas pulp obtained from (prehydrolysis) Kraft is much darker in color depending on respective residual lignin contents. Since cellulose and hemicelluloses appear inherently white, for chemical pulps the bleaching process primarily serves to remove the residual lignin (1.5 – 6%) [80,81] after cooking. As mentioned in section II.I.I, an extension of the cooking process to reduce non-cellulosic impurities leads to cellulose degradation and inevitably reduces the pulp quality. Therefore, various bleaching methods have proven to be effective to continue the delignification process in order to produce high-quality dissolving grade pulps (e.g., chlorination, alkaline extraction, chlorine dioxide, molecular oxygen at high pressure, hypochlorite, peroxide, or ozone). Lignin-preserving bleaching treatments merely

destroy the chromophore structures left in the pulp to achieve a higher degree of brightness afterwards [81,82].

IV Regenerated Cellulose Fibers

Regenerated cellulose refers to a class of materials that primarily includes cellulosic man-made fibers including viscose, Modal, Lyocell (TENCEL™)[3] and also films (cellophane), membranes and sponges. In oder to manufacture regenerated cellulose fibers, dissolving-grade wood pulp has to be dissolved first. Since cellulose itself does not dissolve in most common solvents, it needs to be chemically modified by derivatization in terms of viscose and Modal. In the Lyocell process, wood pulp is directly dissolved in *N*-methylmorpholine *N*-oxide (NMMO) or by using different solvents, (e.g., ionic liquids) [54,83,84].

IV.I Viscose

Viscose generally refers to both viscose fibers for the production of textiles or nonwovens and the solution of cellulose xanthate in caustic soda. Over the past 100 years the production of viscose has evolved into a complex industrial process: Wood pulp or cotton linters are converted in a series of processing steps to a spinnable solution (dope) and then into long filaments with defined length, denier, and cross-sectional shape. To illustrate, the flow diagram in Fig. IV.I shows a typical multi-stage process for viscose with each step allowing to engineer the fiber chemically and structurally [84,85].

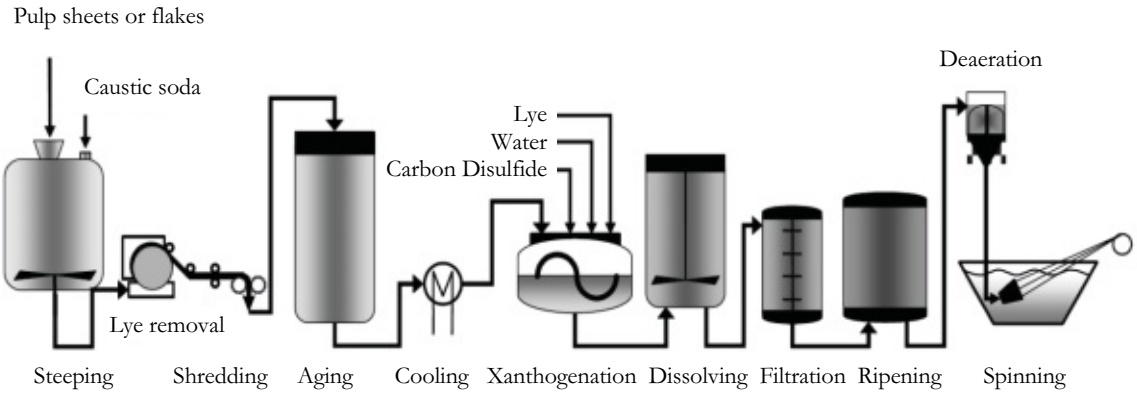

Fig. IV.I Scheme of viscose fiber production according to Lenzing AG (Austria), adopted from A. Rußler [85].

[3] TENCEL™ is a trademark of Lenzing AG

In the first step, dissolving pulp is steeped in an aqueous solution of sodium hydroxide converting the cellulose to sodium cellulosate often referred to as *alkali cellulose*. The treatment causes swelling of the pulp, i.e., the separation of the intermolecular hydrogen bonds increases the accessibility of the hydroxyl groups for subsequent xanthogenation and thus the solubility of the cellulose xanthate [84–86].

Residual hemicelluloses and in particular short cellulose fragments are dissolved in the steeping stage and then removed from the pulp while pressing off the excess lye. After the pressing is completed, the alkali cellulose is shredded to provide adequate surface areas for optimal accessibility to the chemicals and further uniform reactions. The subsequent (pre-)aging or mercerizing is performed under controlled condition of time and temperature to adjust the desired degree of polymerization by oxidative depolymerization, improving the later solubility and spinnability [84–86].

In xanthogenation, carbon disulfide is added to the aged sodium cellulosate to form sodium cellulose xanthate prior to dissolving in sodium hydroxide. A uniform introduction of the xanthate groups within the cellulose is significant for the process considering dissolution and filtration properties. The adjustment and control of temperature (heat of reaction), CS_2 consumption, CS_2 vapor pressure, and the composition of the alkali cellulose (and so its reactivity) are jointly decisive for an effective derivatization. Simultaneous side reactions additionally complicate reaction control during sulfidation. The cellulose xanthate is dissolved in dilute sodium hydroxide to yield a honey yellow- to orange-colored solution – preferably at low temperatures to increase the solubility [84–88].

After filtration, the viscous solution is ripened to the desired coagulation point suitable for spinning. The ripening continues about 18 to 48 hours and thus represents the most time-consuming process step in viscose production. Gradual filtration serves to remove solid particles like undissolved cellulose fibers that otherwise would plug the spinnerets. Like filtration, deaeration is important for continuous spinning, since the formation of gaseous inclusions affects the strength properties as the viscose is extruded into filaments [84,85].

Additives (modifier or spinning aids) and pigments can be added to the viscose dope prior to the spinning process. Surface active components are generally used to slow down the regeneration process. Thus, a higher orientation of the cellulose chains is achieved at stretching.

Often the addition of titianium dioxide pigments is used for the manufacture of dull instead of bright fibers, usually for NW applications [84,85].

The filtrated and deaerated spinning solution is formed into fibers in a wet spinning process, whereby the viscose dope is extruded through a spinneret into a spinning bath formulated from diluted sulfuric acid, sodium sulfate, zinc sulfate, and specific additives, supporting the reformation process of cellulose. Most spinnerets are fabricated from platinum/gold alloys to meet the tremendous requirements regarding the spinning bath. For spinning of various types of fibers, (e.g., staple fibers or filaments) one spinning unit contains a few thousand to 70'000 single holes with diameters in the range of 25 to 250 µm. The design of the spinnerets and the balanced composition of the spinning bath are decisive factors for the structure of the fiber and thus the fiber properties [84,85,89].

The spinning process involves a complex series of physical and chemical reactions that take place almost simultaneously. Initially, the content of sodium sulfate in the acid spinning bath causes the viscose to coagulate. Coagulation is primarily a physical process including dehydration, densification, orientation, and crystallization. The viscose first solidifies into a gel, which initiates the formation of the so-called *skin-core* structure of the filament. As the sulfuric acid diffuses into the filament, the cellulose regenerates from sodium cellulose xanthate with the formation of carbon disulfide and sodium sulfate. However, this follows the transient state of thermodynamically preferred zinc cellulose xanthate complexes in certain regions where additional more complex species also occur, especially when using viscose modifiers. Accordingly, the addition of zinc sulphate in the spinning bath decelerates the regeneration process, thus enabling a higher orientation of the regenerated fibers [84,85].

To achieve acceptable tensile properties, the extruded viscose filaments are further stretched. However, cellulose is not thermoplastic like some plastics, (e.g., polyester) so stretching takes place during or very soon after extrusion, when the structure within the viscose filaments is not yet completely fixed and the cellulose chains can still be aligned. Further post-treatment steps are necessary to obtain a finished product, including several cleaning and bleaching steps and drying. For the production of staple fibers, the viscose filament is fed into a clipper, which cuts the fiber into the desired staple length, usually before cleaning [84,85]. A general post-treatment scheme is shown in Figure IV.II.

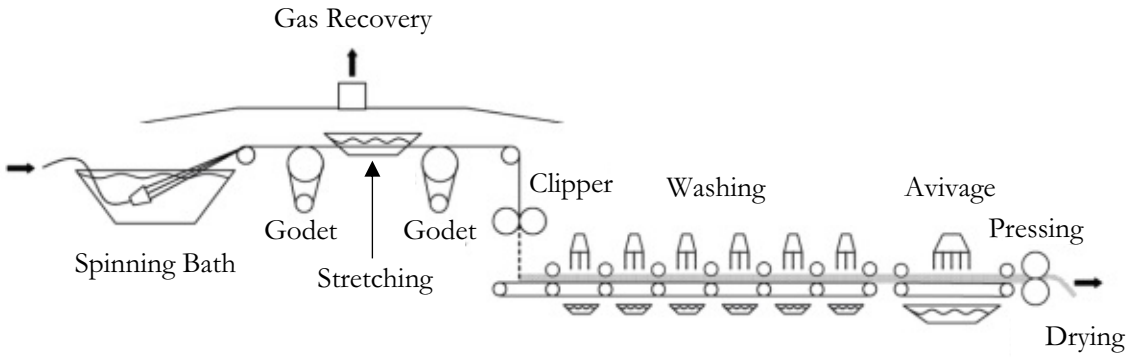

Fig. IV.II Scheme of post-treatment of viscose fiber production according to [84], adopted from A. Rußler [85].

Further textile processing of the fibers (e.g., in spinning and weaving machines) is difficult due to the rough surface of the cellulose fibers. Finishing agents or lubricants, mostly solutions or emulsions of fatty acids and/or derivatives, commonly known as *avivage*, are applied before drying to prevent friction. Antistatic or hydrophobic substances are also used for certain applications [84,85].

As the last production step, the drying process again has a decisive influence on the final fiber properties. During the drying process, the dimension of the fiber changes (shrinkage) and also its molecular structure, which impacts e.g., the water absorbency and dyeability [90–94].

IV.I.I Environmental and Health Aspects

It is already mentioned in section III.I that cellulose needs to be derivatized in the viscose process, i.e., the cellulose is alkalized and dissolved as sodium cellulose xanthate in carbon disulfide, followed by its regeneration as filament or staple fiber in acid solution. In this process, carbon disulfide exposure occurs concomitantly with the exposure to hydrogen sulfide (H_2S), a malodorous highly toxic and flammable gas. In particular, CS_2 is an irritant and metabolic toxicant that vaporizes at room temperature and is readily absorbed by inhalation in man, although skin contact is also possible. CS_2 causes both acute and chronic forms of poisoning. Its vapor forms a highly explosive mixture with air and is spontaneously flammable at 130 – 140 °C. Furthermore, in liquid CS_2, a static electric charge may occur and initiate an explosion. Thus, the greatest caution is required when handling carbon disulfide and must under no circumstances come into contact with an electric charge, spark, flames, or even high temperatures [94–96].

In addition to health problems, CS_2 poses additional dangers for the environment as it is converted to SO_2 and carbonyl sulfides in the lower atmosphere. Thus, the control of toxic and air-polluting compounds like CS_2 in the viscose industry is essential to protect people and environment [95–97].

IV.II Lyocell

Lyocell (or TENCEL™)[4] is first in a new generation of cellulosic fibers. The direct dissolution of the wood pulp without the formation of an intermediate compound differentiates the Lyocell process from other rayon routes. As already mentioned in section III.I.I, the production of viscose fibers results from the use of CS_2, a toxic, flammable, and environmentally sensitive chemical compound, that cannot be recycled after use. The continuous demands for the fiber industry to become more sustainable and economic have driven the development of the Lyocell technology since the first commercial production in 1984 [60,62].

Lyocell manufacturing requires a few numbers of process steps compared to viscose production. The direct dissolution of the cellulose favors this process and ideally NMMO and water can be reprocessed almost completely, e.g., the NMMO recovery in commercial large-scale plants is more than 99%. Thus, the Lyocell process offers an environmentally friendly technology for the industrial production of cellulose fibers [60].

Apart from environmental advantages in processing, the Lyocell fiber proves its high product quality through very high strength properties and excellent tenacity in the wet state. Lyocell fibers can be well blended with natural or synthetic fibers, (e.g., silk, wool, linen, or polyester) and have good thermal resistance and shape stability. However, due to the high degree of crystallinity, the wet fibers show an increased susceptibility to fibrillation [62,98–102].

In order to achieve high quality fiber, comparatively high demands are placed on the pulp quality. In contrast to the viscose process, a modification of certain quality characteristics of the pulp is not feasible as no derivatization occurs. Furthermore, the process is very sensitive to metal compounds and further byproducts (exothermicity), i.e., at elevated temperatures NMMO tends to undergo highly exothermic decomposition catalyzed by the presence of some metal ions [103]. Nevertheless, the flexibility of the process has been sufficiently

[4] TENCEL™ is a trademark of Lenzing AG

optimized with regard to the cellulose material used. Rosenau et al. [60] indicated that paper grade pulp, unbleached chemical pulp, cotton, and viscose fibers, or even cotton waste fabrics (REFIBRA™)[5] can be employed for Lyocell production [104].

A commercial Lyocell process starts from a slurry, a suspension of wood pulp in a 50:50 (w/w) aqueous NMMO solution with the addition of small amounts of antioxidants (e.g., propyl gallate) to prevent cellulose degradation. The dissolution of the cellulose is based on the interaction of the hydrogen bonds between NMMO, water, and cellulose. The oxygen of the strongly N–O dipole in *N*-methylmorpholine *N*-oxide is able to disintegrate the inter- and intramolecular hydrogen bonds within the cellulose. The simultaneous swelling favors the gradual separation of the interfibrillar cellulose structure. Since water and cellulose show a competitive behavior towards hydrogen bonding with NMMO with water being dominant, solutions containing more than 15 – 17% (w/w) water are not able to dissolve cellulose. Thus, excess water is removed under reduced pressure from the ternary system *NMMO/water/ cellulose* to dissolve the cellulose. However, at water concentrations below 4% (w/w) NMMO tends to decompose due to elevated temperatures (72 – 120 °C) required for the dissolution process [60,62,105,106]. According to the ternary phase diagram in Fig. IV.III, the appropriate range for the water content in NMMO is set between 4 and 17% (w/w). The approximate (very small) solubility region of cellulose is highlighted in grey in Fig. IV.III [107].

Ideally, the dissolution procedure of cellulose in NMMO is supposed to be entirely physical causing no chemical changes in the pulp or in the solvent. However, according to Rosenau et al. [60], numerous interrelated chemical processes proceed, involving solvent and the solute cellulose. A complication of the process control is caused by the tendency of NMMO in solution to degrade exothermically, e.g., due to incorrect commissioning or chemical contamination of the solution (copper or iron ions). If an exothermic reaction occurs, the temperature of the solvent increases rapidly and so is the pressure. The decomposition products are volatile amines and water [60,62,103].

Prior to spinning, the filtration of the solution is necessary to remove various impurities out of the solution as undissolved fibers or inorganic compounds may affect the spinnability of the dope. At temperatures around 100 °C, the spinning solution is extruded out from a

[5] REFIBRA™ is a trademark of Lenzing AG

spinneret and spun through an air gap into a dilute NMMO solution where the regeneration of the cellulosic solute takes place. Each spinneret consists of multiple holes with diameters about 4 – 100 µm, designated for the comparatively high viscosity of the solution. In the Lyocell process, the high viscosity of the dope enables very stable spinning of fibers [62,108].

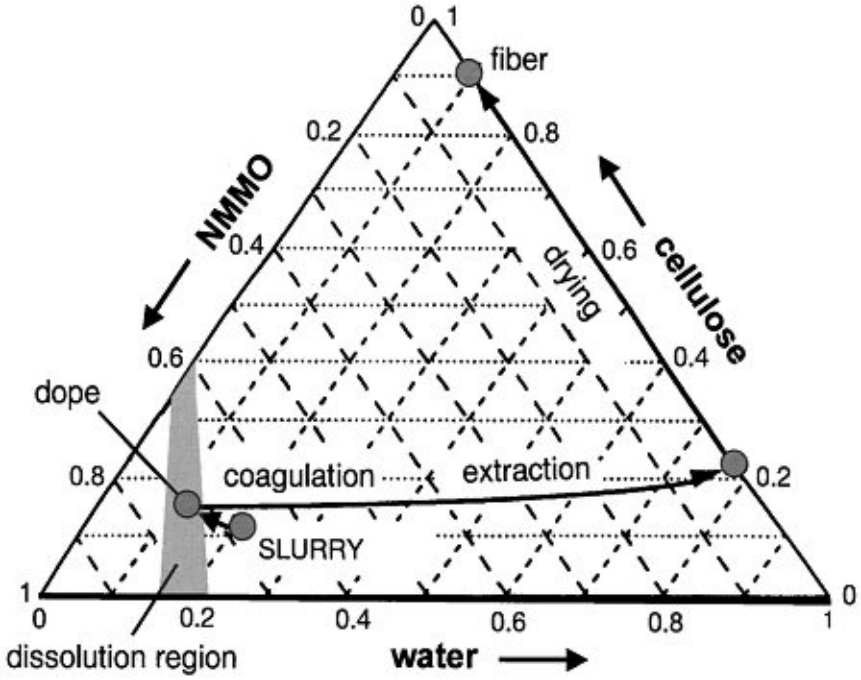

Fig. IV.III Phase diagram of the ternary system NMMO/water/cellulose indicating process steps in Lyocell production at about 100°C [107].

Compared to the viscose process, the extruded filaments pass an air gap (organic solvent dry jet-wet spinning process) and are cooled with a gas flow before they enter the spinning bath. In the Lyocell process, the regeneration of the cellulose proceeds via spinodal decomposition through desolvation with NMMO being exchanged for water. The diffusion rates range here from 10^{-11} to 10^{-9} $m^2 \cdot s^{-1}$, which is sufficient to complete the precipitation of cellulose in a time period of milliseconds to seconds. As result, the chain orientation within the extruded filaments needs to be achieved before entering the spinning bath, which demonstrates the influence of air gap conditions on the structure formation of Lyocell fibers [62,109–111].

To remove remaining NMMO, the fibers are washed with hot demineralized water. The amine oxide solution of the precipitation and washing baths is then recovered and reused as solvent in a close loop system. After washing, the fibers could be bleached if required. Prior to the drying process the avivage is applied to make processing easier, like the viscose fiber

post-treatment mentioned in section III.I. In order to achieve specific fiber properties, further post-treatments (also mentioned for viscose fibers in section III.I) can be carried out [62,112].

IV.III Structure and Properties of Viscose and Lyocell Fibers

Lyocell fibers are clearly different in structure compared to viscose fibers. The longitudinal indentations, which can be seen especially in the cross section of the viscose fibers are due to the regeneration mechanism during the spinning process. In the spinning bath, the external layer of the dope emerging from the spinneret first coagulates. In this way a skin-core structure is formed, which acts as a semi-permeable membrane. The osmotic pressure between the cellulose solution and the precipitation bath then leads to the diffusion of water out of the filament and as a consequence to the folding of the still plastic skin [62,113,114].

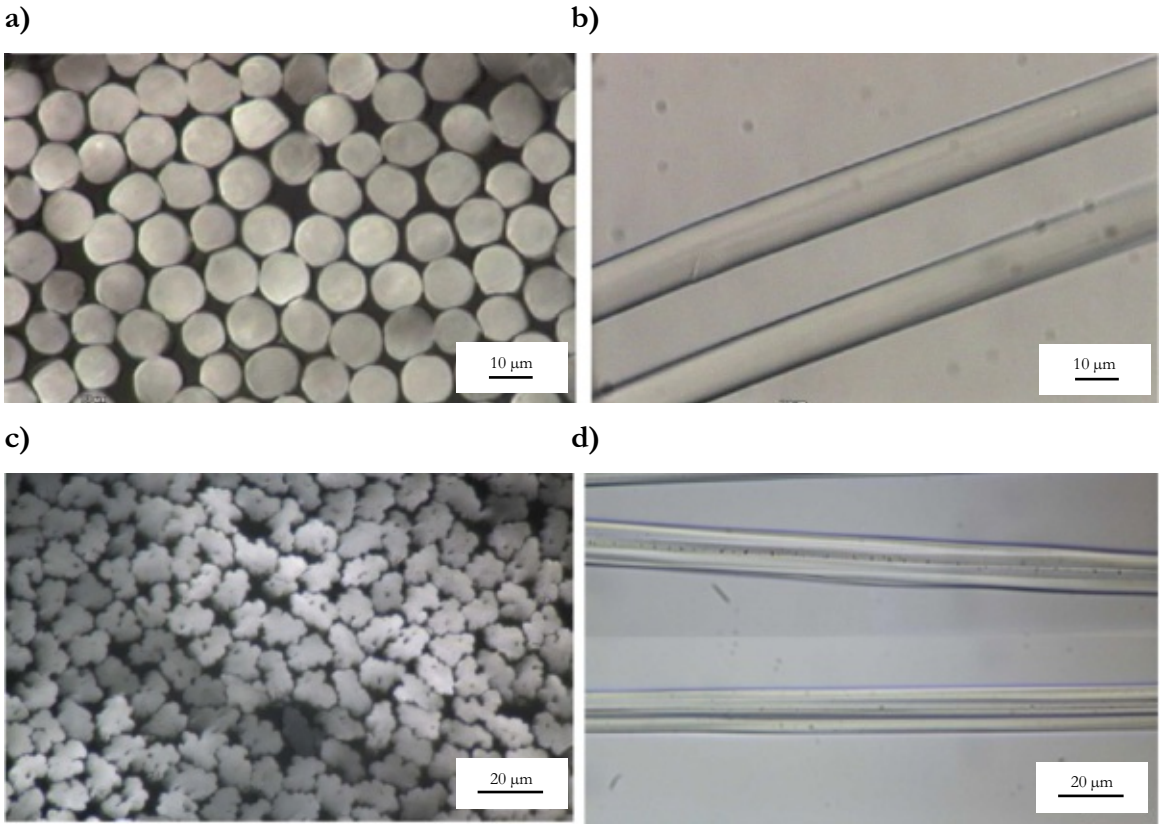

Fig. IV.IV. **a)** Lyocell fiber cross-section and **b)** longitudinal view; **c)** viscose fiber cross-section and **d)** longitudinal view. The pictures were provided by courtesy of Lenzing AG (Austria).

During the dry jet-wet spinning in the Lyocell process, the fibers are oriented and then crystallization occurs. In contrast, Lyocell fibers exhibit a rather smooth fiber surface, a

circular cross-section, and a homogeneous appearance, as well as a dense fibrillar structure. For instance, Mortimer et al. [111] examined the influence of the air gap condition on the formation of fibers from a solution of cellulose in NMMO and water. The core of the Lyocell fibers consists mainly of numerous fibrils arranged along the fiber axis with high orientation in both crystalline and amorphous regions. It appears that a thin skin wraps the inner fibrils together. As a result, Lyocell fibers show higher mechanical properties, higher dry and wet tenacity, as well as higher wet modulus compared to viscose fibers. However, some unexpected fibrillation can also occur around the regenerated fiber surface. [62,108,111,113,115,116]. A comparison of the structural differences is shown in Fig. IV.IV.

The cross section of regenerated cellulose fibers can be modified by adapting the spinning conditions accordingly. This enables the production of fibers with completely new properties and thus opens up new fields of application, e.g., the trilobal cross-section of the viscose fiber (LENZINGViscostar®)[6] offers an enhanced absorption capacity due to the higher fiber surface area of the trilobal cross section, favoring higher water retention without loss in mechanical properties. Due to its absorbent properties, the fiber is particularly suitable for nonwovens in hygiene applications [117].

IV.III.I Fiber Fineness

In addition, the fiber fineness T_t, (i.e., linear density or titer) is an essential property for characterizing man-made fiber materials as a measure of the mass per unit length. A distinction is made between fibers (or staple fibers) and filaments. Filaments are also called endless fibers because they are more or less of infinite length. A filament can be made from a single thread (monofilament) or consists of several threads (multifilament). For the production of staple fibers filaments are cut to approx. 30 – 150 mm.

Fiber fineness is of decisive importance for the physiological properties of textiles and nonwovens. Furthermore, appearance and dyeability depend on it. Man-made cellulosic fibers are usually specified in the internationally recognized unit *tex* or *decitex*, for which the fiber weight in grams is normalized to a length of 1000 m or 10'000 m respectively. The traditional unit *denier* refers to a fiber length of 9000 m and is close in value with decitex.

The corresponding mathematical relationship is given by Eq. (IV.I), where T_t is the linear density (titer) and w_f the corresponding weight of the fiber of known length L_f, where S is

[6] LENZINGViscostar® is a trademark of Lenzing AG

the normalizing factor given each type of unit [118–121].

$$T_t = \frac{w_f \cdot S}{L_f} \tag{IV.I}$$

In the case of cellulosic fibers, an estimate value of 1.5 g/cm^3 is usually used for the material density ρ to determine the fiber diameter d_f according to Eq. (IV.II). The corresponding differences in length and volume dimensions must be taken into account [121].

$$d_f = \sqrt{\frac{T_t}{\pi \cdot \rho \cdot S}} = \sqrt{\frac{T_t}{\pi \cdot 1.5 \cdot S}} \tag{IV.II}$$

V The Zeta Potential

The zeta potential ζ (or electrokinetic potential) is a model parameter used to indicate the charging behavior at interfaces, especially in solid-liquid interactions. The charging behavior at solid-liquid interfaces and the zeta potential are illustrated using the model of the electrochemical double layer (EDL), generally based on the work of *Gouy*, *Chapman*, *Stern* and *Grahame*. If a solid surface is in chemical equilibrium with an aqueous solution, the interfacial charge distribution is different from the charge distribution within the liquid (bulk) phase, i.e., in contact with an aqueous solution an electrical/electrochemical double layer of counterions is formed at the solid-liquid interface to compensate the surface charge [122].
As depicted in Fig. V.I., the EDL consist of a stationary or immobile layer (Stern layer) and a diffusive or mobile layer of ions, where the Stern layer may be divided into a substructure referred to as the inner and the outer Helmholtz planes. The surface charge gives further rise to a surface potential Ψ, which decreases with increasing distance from the solid surface [123].

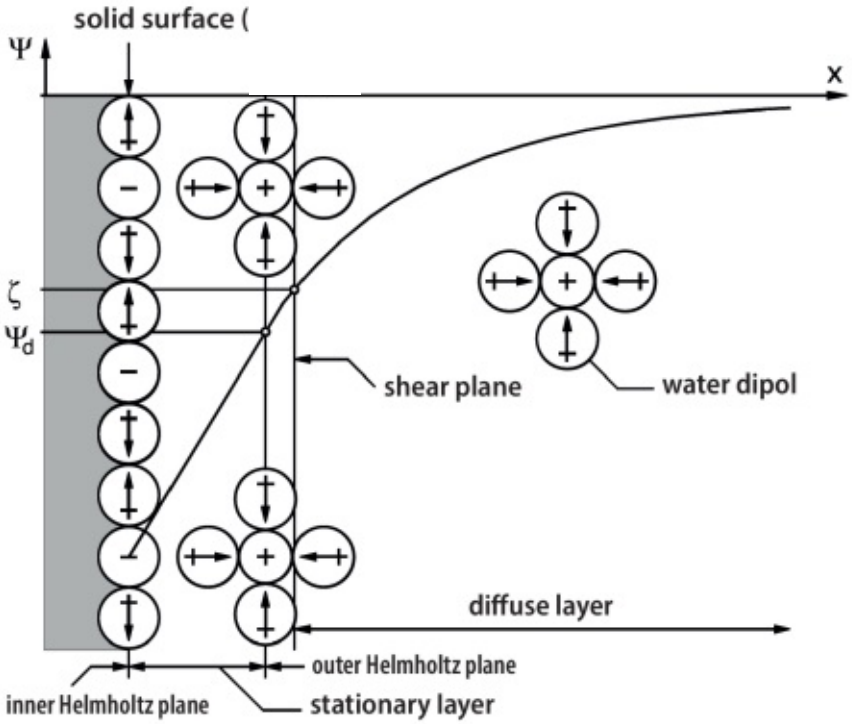

Fig. V.I Model of the electrochemical double layer (EDL) at the solid-liquid interface, adopted from [123].

The zeta potential is defined as the electrical potential at the boundary between the stationary and the diffusive layer of counterions known as *shear plane*. It indicates the location of slipping of the moving liquid phase relative to the stationary layer during the electrokinetic measurement. As an interfacial property, the zeta potential depends on both the surface potential (surface charge) and the properties of the liquid phase. For the investigation of electrokinetically ideal surfaces with e.g., low surface roughness and no porosity or swelling, the position of the shear plane is identical to the outer Helmholtz plane. However, considerable deviations occur when preforming zeta potential analysis of electrokinetically non-ideal surfaces, such as regenerated cellulose fibers [122,123].

V.I Surface Charge Formation

The formation of the surface charge at the solid/liquid interface is based on acid-base reactions between surface functional groups and the aqueous solution and/or the preferential adsorption of (water) ions. Cellulosic materials contain acidic surface functionalities such as carboxylic or hydroxyl groups. The surface charge arises from the protolysis, i.e., the functional groups dissociate in water and remain negatively charged, whereas basic surface functionalities are protonated and assume a positive surface charge. The equilibrium of the surface charge depends on the area density of surface functional groups and, hence, the pH value and the ionic strength of the aqueous solution [122]. However, the determination of the dissociation constants of functional groups in cellulose is rather complex and different pK_a values have been reported for cellulose [1,124–127]. Since cellulose can be considered a polyelectrolyte, the pK_a value itself is dependent on the neighbor electric charges in the chain and in the medium. Nevertheless, the kinetics of cellulose degradation in alkaline solutions must be taken into account [128].

Even in the absence of functional groups, hydrophobic surfaces acquire an interfacial charge and thus a zeta potential. Preferential adsorption of hydroxide ions (OH^-) has been suggested as source of surface charge formation at the solid-liquid interface for non-ionogenic, assuming that OH^- ions behave more hydrophobically than hydronium (H_3O^+) ions. According to this process, the surface charge and thus the zeta potential depend on the pH of the aqueous solution. At high pH the surface will acquire a negative electrokinetic potential due to the presence of OH^- ions, whereas the concentration of H_3O^+ ions becomes more dominant with decreasing pH.

Based on a different model, the formation of a "virtual" surface charge relies on polarization effects of the hydrophobic solid surface on the water molecules, but the charging behavior

at the solid-liquid interface again strongly depends on the pH of the aqueous solution and the effect on the zeta potential remains the same [122].

V.II The Streaming Potential Technique

As describes in the previous section, the zeta potential is defined as the electric potential at the shear plane between the stationary layer and a mobile layer of charges. The zeta potential is determined by measuring an electrokinetic effect, whereby the relative movement between an electrolyte solution and a charged solid surface is caused by either a mechanical or an electrical driving force. Among several techniques, the streaming potential technique (or alternatively the streaming current method) is most suitable for solid surface zeta potential analysis. In this context, the zeta potential refers to the charging behavior at the macroscopic solid-liquid interface [122,123]. Electrokinetic phenomena, (e.g., electrophoretic mobility, electro-osmotic flow, and electrokinetic sonic amplitude) where the driving force is applied by an electric field, assess the zeta potential of colloidal dispersions of particles and liquids, and are discussed in detail elsewhere [129].

If a tangential flow of liquid is generated across a solid surface when an aqueous electrolyte solution is forced through a capillary system, (e.g., a porous plug of fibers) by means of hydraulic pressure, the counterions compensating the surface charge in the diffuse layer are moved in the direction of flow due to Stoke's friction. In an electrically non-conductive capillary system, the resulting streaming current leads to the formation of a potential difference. The charge separation generates an electric field that forces a back-current of charges which partially compensates the streaming current in flow directions. In equilibrium condition, the streaming current is equal to the incipient back-current and the appearing potential difference is referred to as streaming potential. A term for the calculation of the zeta potential ζ (usually in millivolt) from streaming potential measurements is given by the Helmholtz-Smoluchowski equation [122,123]:

$$\zeta = \frac{dU_{str}}{d\Delta p} \cdot \frac{\eta}{\varepsilon_r \cdot \varepsilon_0} \cdot \frac{L}{A} \cdot \frac{1}{R} \qquad \text{(V.I)}$$

In this Eq. (V.I) the measured streaming potential coefficient $\frac{dU_{str}}{d\Delta p}$ is related to $\frac{L}{A}$ the cell constant of the sample. U_{str} is the induced streaming potential at a constant pressure difference Δp and R is the electrical resistance within the streaming channel. η is the dynamic

viscosity of the electrolyte solution, where ε_r is its relative permittivity (dielectric constant) and ε_0 is the permittivity of free space. With this approach, the zeta potential is metrologically defined. In theory, a linear dependence of the streaming potential (or streaming current) on the pressure difference is assumed. It proves to be advantageous to record the streaming potential at continuously variable pressure difference, i.e. a defined pressure ramp is set individually for the analysis. Thus, in zeta potential analysis the streaming potential coefficient is interpreted as the gradient of the recorded straight line, where U_{str} is plotted over Δp [122].

The cell constant consists of two parameters, i.e., the length L, and the cross-sectional area A of the streaming channel that cannot be determined easily for samples of complex geometry, such as plug of randomly oriented fibers. For irregularly shaped samples where the geometry of the streaming channel is not accessible a derivative of the Helmholtz-Smoluchowski equation is applicable, using the definition of the electrical conductivity κ:

$$\kappa = \frac{1}{R} \cdot \frac{L}{A} \tag{V.II}$$

Since the electrical conductivity κ within the streaming channel cannot be measured directly, it is a valid approach for non-conducting samples to replace κ by the conductivity of the bulk electrolyte solution κ_{bulk}. Eq. (V.I) can be replaced by:

$$\zeta = \frac{dU_{str}}{d\Delta p} \cdot \frac{\eta}{\varepsilon_r \cdot \varepsilon_0} \cdot \kappa_{bulk} \tag{V.III}$$

However, Eq. (V.III) neglects the possible occurrence of interfacial surface conductivity or related conductivity effects contributed by the solid sample. The surface conductivity leads to an increased electrical conductivity within the streaming channel compared to the bulk solution. The zeta potential calculated according to Eq. (V.III) thus refers to a smaller (electrolyte) conductivity and is therefore rated too low. It is denoted as the "apparent" zeta potential. In oder to obtain the correct or "real" zeta potential various methods have been introduced in the literature to compensate the effect of the increased conductivity within the streaming channel compared to the bulk conductivity [122].

The approach of Fairbrother and Mastin [129] determines the cell constant $\frac{L}{A}$ according to Eq. (V.II) by measuring the electrolyte conductivity κ_{high} and cell resistance R_{high} at high ionic strength.

$$\zeta = \frac{dU_{str}}{d\Delta p} \cdot \frac{\eta}{\varepsilon_r \cdot \varepsilon_0} \cdot \frac{1}{R} \cdot \kappa_{high} \cdot R_{high} \qquad \text{(V.IV)}$$

With this approach, it is assumed that additional conductivity effects introduced by the solid sample are suppressed with increasing conductivity of the electrolyte solution. The correction equation of Fairbrother and Mastin is primarily applicable to compensate the influence of the surface or interfacial conductance, but it may be invalid for other conductivity sources, (e.g., electronic, or ionic conductivity of the solid sample) or complex sample systems such as fibers [122,131].

V.III Dependences of the Zeta Potential

The charge formation at the solid-liquid interface has been explained by two different mechanisms in section V.I. Since both acid base reaction of surface functional groups and the physical adsorption of water ions depend on the pH of the aqueous solution, it is important to take into account the pH dependence of the zeta potential in the measurements. In particular, the isoelectric point (IEP) is a strong indicator for the chemical composition of the sample surface, i.e., for the present surface functional groups, or specific ion adsorption. Depending on whether a material surface has acidic, basic, or amphoteric properties, a characteristic curve of the zeta potential becomes significant when recorded over a certain pH range. Even for zeta potential measurements on hydrophobic surfaces a strong dependence on the pH value of the electrolyte solution is observed. The charge formation on hydrophobic surfaces is attributed to the described adsorption of water ions and it appears that the equilibrium surface concentration of adsorbed charge carriers (hydroxide and hydronium ions) is at pH 4 [132,133]. Therefore, the localization of the IEP of material with hydrophobic surface character (e.g., polymers) at pH 4 is expected [122].

Irrespective of the chemical properties of the material surface, the magnitude of the zeta potential decreases with increasing concentration of the electrolyte solution. This dependence of the electrokinetic potential on the ionic strength is commonly related to the compression of the electrochemical double layer at high ionic strength. If the zeta potential

analysis is limited to the use of a 1:1 electrolyte such as sodium chloride (NaCl) or potassium chloride (KCl), the extension of the EDL can be expresses by the Debye length κ^{-1}:

$$\kappa^{-1} = \sqrt{\frac{\varepsilon_r \cdot \varepsilon_0 \cdot k_B \cdot T}{2 \cdot N_A \cdot e^2 \cdot I}} \qquad \text{(V.V)}$$

Where I is the ionic strength of the electrolyte solution, k_B is the Boltzmann constant, N_A is the Avogadro number, e is the elementary charge and T is the absolute temperature. Due to the specific interactions of multivalent ions with the solid surface, the applicability of this equation is limited to 1:1 electrolyte solutions i.e., the decrease in the magnitude of the zeta potential with increasing ionic strength deviates when using a complex solute, e.g., 2:1 or 3:1 electrolytes [122].

In general, the zeta potential analysis is considered to be independent of the sample size provided that the solid sample does not exhibit complex properties such as porosity, intrinsic conductivity, surface roughness, or swelling [122,131].

Furthermore, a reliable measurement of the streaming potential requires an equilibrium state of the EDL between the solid surface and the surrounding electrolyte solution, whereby the required time for equilibration strongly depends on the solid material. Therefore, this time-dependence of the system must be taken into account, especially in case of running pH or concentration changes in the electrolyte during the measurement. Although individual measuring parameters for the calculation of the zeta potential are dependent on the temperature, a significant effect of temperature on the zeta potential is not observed [122].

V.IV Zeta Potential Analysis of Regenerated Cellulose Fibers

Regenerated cellulose fibers have a crystalline/amorphous structure, which is retained independently of the conversion of the cellulose in solution and further fiber formation processes. The fine structure of regenerated cellulose fibers is schematically shown in Fig. V.II. As indicated in section II.II.II, cellulosic fibers consist of elementary fibrils composed of a network of crystallites (A) and intermediate less-ordered amorphous regions (B). Additional regions, where crystallites are fused to large aggregates (C) and where adjacent amorphous regions are laterally connected (D), including voids (E), complement the fiber structure.

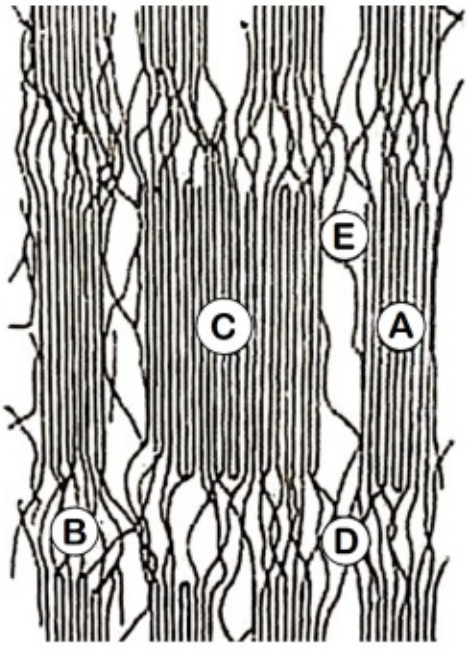

Fig. V.II Fine structure of regenerated cellulose fibers (schematically): **A**, crystallistes; **B**, amorphous regions; **C**, cluster formation; **D**, interfibrillar tie molecules; **E**, voids, adopted from [134,135].

Amorphous regions and the inner surface area of voids are decisive for the accessibility, reactivity, and adsorption properties of fibers. Their physiochemical peculiarity makes cellulosic fibers highly accessible for water and gives them a pronounced hydrophilic character [10]. A significant factor regarding the adsorption properties of fibers is the presence of accessible hydroxyl and carboxyl groups and the proportion of amorphous regions and voids, as there is no water penetration into the highly crystalline regions. The competing interaction of the water molecules with the cellulose (adsorption process) breaks the intermolecular hydrogen bonds between the less-ordered cellulose chains, which causes significant swelling of the fiber [10,122,131].

This swelling capacity of cellulosic fibers has significant effect on the zeta potential. Cellulosic fibers are inherently negatively charged, due to the presence of acidic surface functional groups e.g., carboxyl and hydroxyl groups. When an aqueous solution flows through a plug of randomly oriented cellulosic fibers, it penetrates into the porous fibers and causes an interfibrillar swelling of the surface layers. The incorporation of water molecules extends the fiber surface and shifts the shear plane of the EDL towards the mobile liquid phase [10]. This effect leads to a reduction of the magnitude of the zeta potential. Fig. V.III shows a schematic representation of the shift of the electrokinetic shear plane, (i.e., the location of the zeta potential is defined) in the water-swollen state [10,122].

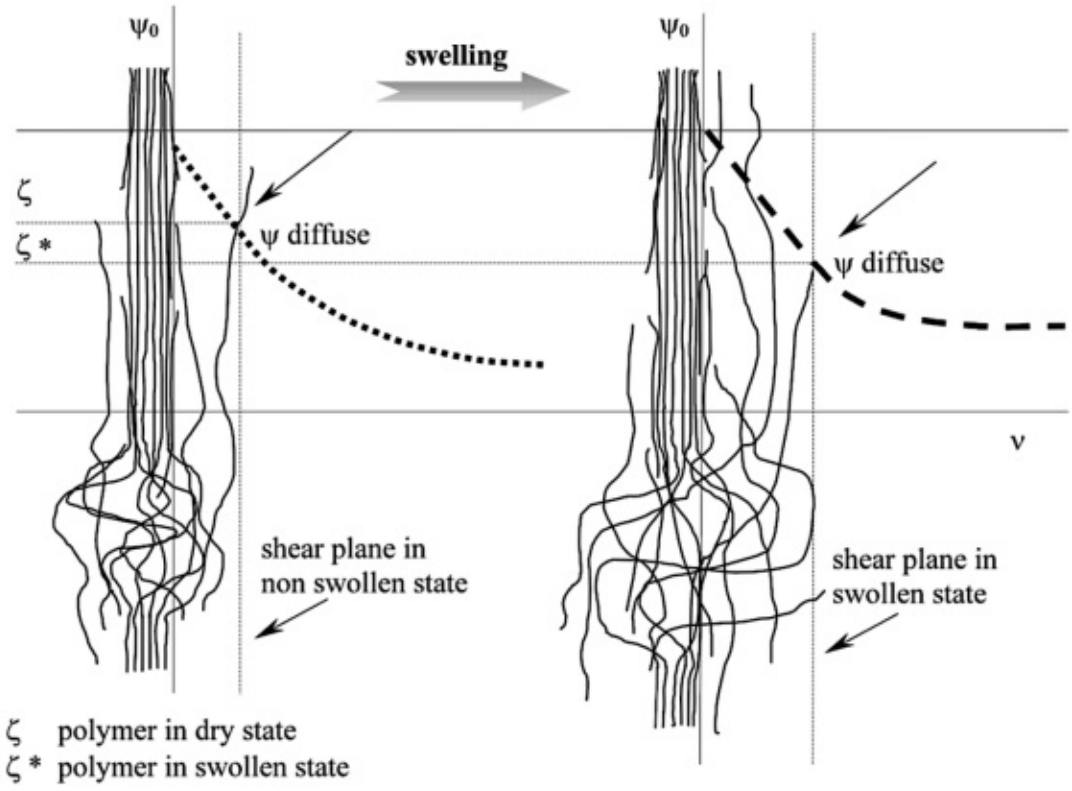

Fig. V.III Reduction of the magnitude of the zeta potential caused by swelling of the fibers in contact with water according to [10].

Furthermore, the uncharged water molecules not only refrain from participation in the process of interfacial charge formation, but also shield the contribution of dissociated surface functional groups [131]. The penetration of the aqueous electrolyte solution additionally increases the ionic conductance within the fiber plug regarding streaming potential measurements, which clearly exceeds the bulk electrolyte conductivity [131]. As discussed in section V.II, inserting the comparatively too low bulk conductivity into Eq. (V.III) distorts the calculation of the "real" zeta potential, especially for electrolyte solutions with low ionic strength.

In general, the swelling behavior of regenerated cellulosic fibers is determined by the molecular and super molecular structure of cellulose. Since the interaction of a solid surface with an aqueous electrolyte solution depends, among other things, on the pH value, the ionic strength, and the chemical composition of the electrolyte solution, it also influences the adsorption properties of cellulosic fibers. Nevertheless, when comparing zeta potentials analysis of different regenerated cellulosic fibers, the structure of voids proves to be more important than other structural characteristics in terms of sorption properties [10].

The complex behavior of cellulose fibers in contact with an aqueous solution presents a challenge for zeta potential analysis. However, the swelling characteristics of cellulose fibers per se may be of interest for the investigation.

VI Materials and Methods

VI.I Sampling and Preparation

Different staple fiber samples were provided by Lenzing AG (Austria) for surface charge analysis. The investigation mainly covered the two most common types of regenerated cellulose fibers Lyocell (CLY) and viscose (CV). In table VI.I., the specifications and structure characteristics from all fibers taken into account for measurements are present. With the exception of special treated samples, the fibers were taken directly from the production process after washing but before the application step for finishing agents (avivage). Following the sampling, the fibers were hermetically sealed and stored at room temperature (20 to 25 °C) between measurements. In this case the fiber is called *never dried* because the fiber has not been subjected to any drying process. Since the sampling was also carried out before the finishing agent bath (avivage), the fiber can be indicated as *never dried before avivage*.

Table VI.I: The specification and characteristics of investigated regenerated cellulose fiber samples

Designation	**Linear density** T_t (dtex)	**Fiber length** l (mm)	**Description**
CLY-NDBA	1.7	38	Standard lyocell fiber; bright
CV-NDBA	1.3	38	Standard viscose fiber; bright
CV-NW-NDBA	1.7	40	Viscose fiber; bright; for NW applications
CV-trilobal-NDBA	3.3	30	Viscose fiber; bright; trilobal fiber cross-section
CLY-0.1%AKD[7]-DS	1.7	38	Lyocell fiber; dull; hydrophobic
CV-0.1%AKD-DS	1.7	40	Viscose fiber; dull; hydrophobic
CV-15%KA1-DS	1.3	38	Viscose fiber; bright; 15% cationic additive 1
CV-18%KA1-WA-DS	1.3	38	Viscose fiber; bright; 18% cationic additive 1; without avivage
CV-20%KA1-DS	1.3	38	Viscose fiber; bright; 20% cationic additive 1
CV-20%KA1-6%KA2-DS	1.3	38	Viscose fiber; bright; 20% cationic additive, 6% cationic additive 2
CV-25%KA1-DS	1.3	38	Viscose fiber; bright; 25% cationic additive 1

[7] AKD = Alkyl ketene dimer

The abbreviation (NDBA) refers to this context in the following text. For initial trials, similar fibers *never dried after avivage* (NDAA) as well as *dryer samples* (DS) were tested additionally but should only mentioned here for the sake of completeness.

Due to the fact that the fibers were taken directly out of the current process, the appropriate selection of samples was determined by, inter alia, the company's production plan. Furthermore, special fibers from earlier experiments were already present in their *dried state* (DS). Nevertheless, these exceptional fiber characteristics were of great interest regarding surface charge analysis.

Besides the fiber samples, there was an additional approach to perform the surface charge analysis of the alkali cellulose - termed as an intermediate in viscose production where beech hardwood pulp is treated with caustic soda. Thus, the alkali cellulose was taken directly from viscose production at Lenzing AG in Lenzing (Austria). For sample preparation it was necessary to wash these strongly alkaline (pH = 12) pulp lumps neutrally. As pulp is not sufficiently stable in this mercerized form, samples were measured immediately after the washing process to prevent degradation.

VI.II Instrumentation

Measurements were performed with SurPASS™ 3 from Anton Paar GmbH heading in Graz; Austria. The device is used for macroscopic solid surface charge analysis enabling fully automated zeta potential analysis in real-life conditions. The instrument was used in combination with an integrated titration unit to investigate the zeta potential stepwise over a selected pH range. This application proves to be useful in determining the isoelectric point of a sample surface. A picture is provided with kind permission of Anton Paar GmbH in Fig. VI.I

Together with the instrument a software for the remote control of the SurPASS™ 3 was provided.

With SurPASS™ 3 electrodes are already mounted in the instrument. For conductivity monitoring a conductivity electrode (WTW TetraCon 235) with temperature sensor was in use.

Fig. VI.I SurPASS™ 3; electrokinetic analyzer for zeta potential analysis of macroscopic solids with additional titration unit (Anton Paar GmbH).

The following information on the instrument and its functionality are in accordance with the recommendations of the "Reference Guide for SurPASS™ 3 and SurPASS™ 3 Eco" by Anton Paar GmbH, Austria [136]. General explanation of the principle of the streaming potential method for zeta potential analysis is based on the work of T. Luxbacher, described in his "Zeta Guide" [122].

VI.II.I Measuring Principle

For direct solid/liquid interface analysis the SurPASS™ 3 is based on the streaming potential and streaming current method. Initially, an aqueous electrolyte solution flows through the measuring cell with the brought in fiber sample. The flow resistance is adjusted manually to generate a pressure difference between inflow and outflow of the measuring cell while the electrolyte solution is passing through the permeable fiber plug. This electrolyte flow causes an electrical charge separation along the measuring cell, resulting in potential difference (streaming potential) or electrical current (streaming current). These two electrical responses are detected by corresponding electrode systems at the inlet and the outlet of the measuring cell. The volume flow is generated by pressurization of the fluid tank with either atmospheric air or inert gas, followed by pressure equalization. During a measurement the streaming potential ΔU_{Str} or streaming current ΔI_{Str} is rerecorded with continuously decreasing pressure difference Δp across the measuring cell (pressure ramp).

Samples of irregular shape (e.g., voids between the fibers in a mounted fiber plug) represent in themselves a capillary system. Therefore, the streaming potential and streaming current analysis for fibers is performed in permeation mode. Appropriate design and geometry of the provided measuring cell ensures that each individual sample is sufficiently permeable for the liquid flow and offers also enough flow resistance to obtain a reasonable pressure difference [122]. Fig. VI.II illustrates the permeation mode for streaming potential and streaming current analysis.

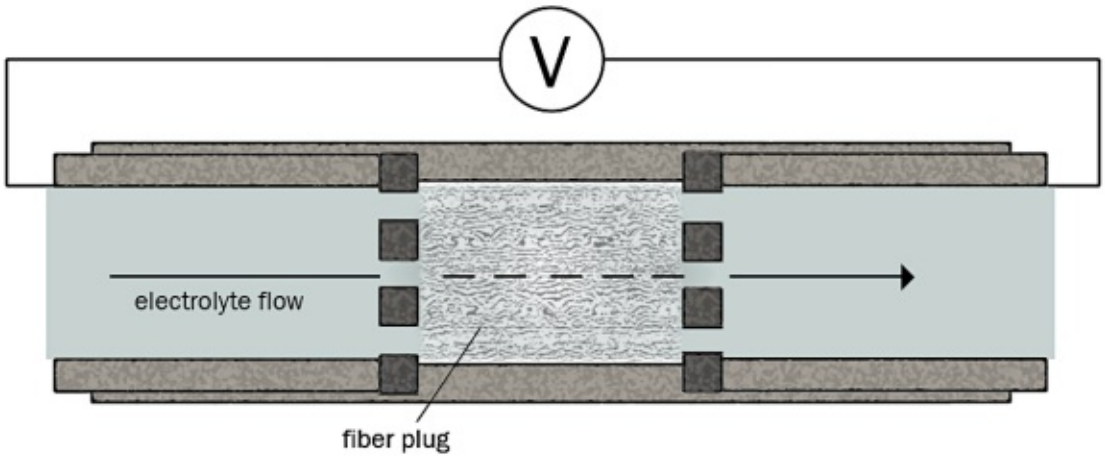

Fig. VI.II Illustration of the permeation mode for streaming potential and streaming current analysis, adopted from [122].

VI.II.II Measuring Cell

To achieve measurements on fibers, granular or powder samples the SurPASS 3 Cylindrical Cell was in use. Depending on the respective fiber moisture, a quantity of 0.3 to 1 g fiber sample was weighed out. In order to ensure the reproducibility of the measurements, the fibers were placed in a particular prescribed measuring cell setup. The fiber sample was filled into the cavity of upper part of the measuring cell and fixed with a liquid-permeable support disk on the top. From below, a previously inserted piston could be used to compress the fiber bundle by pushing it forward gently. This upper part was placed on the lower part of the Cylindrical Cell and fixed with two screws. To adjust the permeability of the sample later, the knob (micrometer screw) was screwed slightly onto the thread of the piston. Finally, the measuring cell was mounted on the instrument. A picture of the Cylindrical Cell is provided with kind permission of Anton Paar GmbH in Fig. VI.III.

Fig. VI.III Components of SurPASS 3 Cylindrical Cell for fibers, granular and powder samples (Anton Paar GmbH).

For measuring fibers *with avivage* the Cylindrical Cell using the sample holder for powders proved to be better applicable. The design of the sample holder allows the formation of a fiber plug with defined permeability. Thus, the adjustment of the permeability during the rinsing cycle can be omitted. Hence the permeability of the fiber plug correlated with the weighed sample quantity. To evaluate the required amount of fiber, between 0.05 an 0.07 g of fibers material was mounted into the sample holder. This measuring set-up was considered due to the supposed water solubility of the avivage components and therefore to avoid contamination of the electrolyte and changes of the outermost layer of the fiber surface. For the investigation of alkali cellulose, the same sample holder was used by reason of its pulpy morphology.

VI.II.III Measurement Conditions and Calibration

Since the zeta potential analysis may be affected by contaminations, high purity chemicals are mandatory for successful measurements. According to the crucial requirements for water quality compiling with the ASTM I[8], only ultrapure water type 1 from Milli-Q® IQ water

[8] American Standard for Testing and Materials I

purification systems was in use. This includes the preparation of electrolyte solutions and titrants as well as the cleaning steps of the entire measuring equipment. Once the measurements were finished, the electrolyte system of the instrument was cleaned with the cleaning device mounted.

The inorganic salts used for this purpose were at least *pro analysi*, or *analytical grade*, to avoid contaminations and to ensure reliable electrolyte concentrations. The solutions were freshly prepared each day and exchanged after each measurement. To prevent absorption of CO_2 the electrolyte solution was continuously purged with nitrogen 5.0 during measurements. The operation pressure was set to 6 bar at the double-stage gas valve of the gas cylinder to reduce the primary pressure.

For the titrants, volumetric solutions (Titrisol®; Merck) were prepared by diluting the concentrate accordingly. Acid (HCl) and base (NaOH) solutions for the titration unit were exchanged after every week.

To maintain a reliable monitoring system, the pH electrode was calibrated once a week with three buffer standard solutions of known pH value, covering measuring range (pH 2, pH 7, pH 10). If not in use, the electrode was stored in 3 mol/l KCl solution. The single point calibration of the conductivity electrode was required once a month with a conductivity standard solution. At the beginning of each measurement the electrodes were cleaned with ultrapure water and wiped off with a lint-free cloth before inserted into the electrolyte solution.

In oder to determine reliable working conditions, a verification measurement was performed when the instrument was put into operation. A standard cotton fabric was folded and mounted in the center of the sample holder of the specific measuring cell. The verification measurement for zeta potential was carried out with 0.01 mol/l KCl standard solution according to the conditions specified in the instruction manual. Since the results met the specific range of the zeta potential of the cotton fabric standard, thus, the reliability of the instrument could be confirmed.

VI.II.IV Measurement Procedure

In oder to perform a successful zeta potential analysis on fibers, the implementation of what has been said so far is a prerequisite. 150 to 200 ml of the prepared electrolyte solution was

filled into the glass beaker including a magnetic stir bar. The pH and conductivity electrodes were put into the respective holder that was covering the glass beaker for monitoring the electrolyte solution. Before starting the experiment, the gas supply was switched on for purging the electrolyte solution constantly with nitrogen. The corresponding burette tips for dosage of acid and base from the titration unit should be inserted in the beaker correctly. Once the sample has been mounted into the corresponding measuring cell set-up, it can be mounted on the instrument and the experiment can be defined in the software.

While rinsing the system three to five times with electrolyte solution the permeability index of the fiber plug was approximately adjusted to 100 by turning the micrometer screw. In order to ensure an equilibrium condition for correct zeta potential analysis during the experiments, the pressure ramps need to overlapp after finishing the rinse cycles. If there was no overlapping observed from the measuring view, the measurement was stopped, and a higher number of cycles was used to reach equilibrium conditions.

A single or series of zeta potential measurements at defined electrolyte composition could be performed typing a certain number of measurements in the selected *zeta potential* measurement field. Changing the pH value of the electrolyte solution could be achieved by selecting the *dosage* task to either *acid* or *base* until a certain pH value is reached. If starting a new zeta potential measurement after changing the pH value of the electrolyte solution at least two rinse cycles have to be performed to reach equilibrium conditions.

To perform zeta potential analysis in a determined pH range automatically, the measurement type "pH scan" intended for this purpose was selected in the software menu. Various parameters for the measurement (e.g. rinse cycle, zeta cycle, pH step, end pH value) can be set there. The instrument is able to execute up to a number four repetitions of zeta cycles at the adjusted pH value. To ensure a sufficient statistic evaluation of the data, three to four *zeta potential cycles* were set for the measurement at each pH increment.
It was important to set at least three *rinse cycles* to ensure sufficient equilibrium conditions between each pH step during the measurement. Both the *end pH value* and the *pH increment* for the scanning procedure were defined before the start. The *start pH value* required for the experiment was previously set via *dosing* function. Once the experiment has been started, the measurement routine can be followed on the monitor, where the zeta potential is plotted against the pH value.

Before starting a pH scan, it is important to make sure that the titration hoses are filled with acid and base sufficiently and all parameters are set correctly. The electrolyte solution should also be flushed with nitrogen. Depending on the size of the selected increment and the width of the pH range to be scanned, a measurement can take up to several hours. Therefore, a suitable time schedule for pH scan experiments should be considered.

Another important parameter for a successful zeta potential analysis is the pressure range. The values for start pressure (600 mbar) and stop pressure (200 mbar) were default values. It proved to be advantageous to increase the value of the start pressure to 800 mbar, in order to eliminate impairments of the experiment (e.g., appearance of air bubbles).

For each performance of reliable zeta potential analysis, the corresponding pressure ramp (streaming potential against pressure difference) is expected to be linear. Deviations become noticeable mainly at the beginning of the decreasing pressure ramp or were caused by air inclusions in the fiber plug, high ionic strengths, and strongly acidic pH values (around pH 2), or strongly basic pH values (>10). To achieve a better correlation for the calculation of the zeta potential, a specific *pressure bar* was set at 450 mbar. Thus, only the recorded data between 200 and 450 mbar were used for calculation. Furthermore, this limitation to a sufficiently wide pressure range was favored by extending the starting pressure to 800 mbar.

Each time an experiment was finished, the system was emptied before demounting the Cylindrical Cell from the instrument. For this, a specific task “empty the system” is listed in the cleaning procedures of the program. The nitrogen flush also is switched off. After emptying the system, the measuring cell could be removed and cleaned to be ready to prepare further experiments.

In oder to achieve reliable results between different experiments, an appropriate cleaning of the system is essential. Whenever a new fiber sample was intended to be measured, the system was cleaned with ultrapure water. Instead of the Cylindrical Cell the Cleaning Cell (especially provided for the cleaning routine) was mounted on the device. The empty and properly cleaned 250 ml glass beaker for aqueous solutions was filled with 200 ml ultrapure water and the cleaning process was selected in the listed cleaning procedures. After cleaning the beaker was cleaned and filled with fresh electrolyte solution, or dried, if the device has to be switched off.

VI.III Preparation of Electrolyte Solutions

Based on the experiences and research of T. Luxbacher the recommended ionic strength of solid surface zeta potential analysis is 0.001 mol/l while using a 1:1 electrolyte. With regard to this reference the majority of measurements were carried out with a 0.001 mol/l potassium chloride (KCl) background electrolyte solution. An aqueous solution containing chloride ions is preferred since the use of Ag/AgCl reference electrodes [137,138].

To prepare the stock solution, 0.9319 g KCl (M_{KCl} = 74.5513 g/mol) were weighed into a 250 ml volumetric flask and filled up with ultrapure water. As soon as the salt has been completely dissolved under repeated shaking, 5.000 ml of the clear solution were transferred with an Eppendorf® Repeater™ M4 into another 250 ml flask and filled up to the mark with ultrapure water again.

By suppling an electrolyte solution with defined ionic strength its effect on the reproducibility of the streaming potential and streaming current measurement can be eliminated. Thus, the preparation of the electrolyte solutions requires a high degree of accuracy and clean laboratory equipment. To additionally prevent the introduction of foreign ions, the glassware was cleaned exclusively by hand and rinsed several times with ultrapure water afterwards. Nevertheless, the application of the streaming potential and streaming current method considering the dependence of the zeta potential on the ionic strength is of certain interest. Besides the use of an aqueous solution with a 1:1 electrolyte (KCl) the dependence of the zeta potential on the ionic strength was investigated with multivalent ions too.

For measurements with salt solutions of different valency and varying ionic strength, 250 ml stock solutions with an ionic strength of 0.9 and 0.09 mol/l out of each salt were prepared. Further solutions with ionic strengths of 0.009, 0.0009 and 0.00009 mol/l could be made from these stock solutions afterwards. For this purpose, 2.500 ml of each solution conforming to 100 times the requested ionic strength was transferred with an Eppendorf® Repeater™ into a 250 ml volumetric flask and filled up with ultrapure water. Following this procedure, dilution series for potassium chloride (KCl), calcium chloride ($CaCl_2$), magnesium chloride ($MgCl_2$) and aluminum chloride ($AlCl_3$) were prepared according to the scheme in table VI.II.

Concentrations of 0.05 mol/l acid and base were prepared for the titration unit. Hydrochloric acid was used as acid and NaOH as base.

Table VI.II: Compilation of the prepared electrolyte solutions and chemicals used for the analysis of the dependence of the zeta potential on the ionic strength

Stock solution (250 ml)					
Electrolyte		Ionic strength (mol/l)	Concentration (mol/l)	Weighted sample (g)	Salt used for preparation
KCl	SS1	0.9	0.9	16.7736	KCl, 99.5-101.0% CAS Number: 7447-40-7 *VWR Chemicals*
	SS2	0.09	0.09	1.6774	
$CaCl_2$	SS1	0.9	0.3	8.3235	$CaCl_2$, anhydrous ≥ 96% CAS Number: 10043-52-4 *VWR Chemicals*
	SS2	0.09	0.03	0.8324	
$MgCl_2$	SS1	0.9	0.3	7.1415	$MgCl_2$, anhydrous ≥ 98% CAS Number: 7786-30-3 *VWR Chemicals*
	SS2	0.09	0.03	0.7152	
$AlCl_3$	SS1	0.9	0.15	9.0536	$AlCl_3 \cdot 6H_2O$ ≥ 99% p.a. CAS Number: 7784-13-6 *Honeywell Chemicals*
	SS2	0.09	0.015	0.9054	
Dilution series (250 ml)					
Electrolyte		Ionic strength (mol/l)	Concentration (mol/l)	Stock solution used for preparation (2.500 ml)	
KCl	SS3	$9 \cdot 10^{-3}$	$9 \cdot 10^{-3}$	KCl – SS1	
	S4	$9 \cdot 10^{-4}$	$9 \cdot 10^{-4}$	KCl – SS2	
	S5	$9 \cdot 10^{-5}$	$9 \cdot 10^{-5}$	KCl – SS3	
$CaCl_2$	SS3	$9 \cdot 10^{-3}$	$3 \cdot 10^{-3}$	$CaCl_2$ – SS1	
	S4	$9 \cdot 10^{-4}$	$3 \cdot 10^{-4}$	$CaCl_2$ – SS2	
	S5	$9 \cdot 10^{-5}$	$3 \cdot 10^{-5}$	$CaCl_2$ – SS3	
$MgCl_2$	SS3	$9 \cdot 10^{-3}$	$3 \cdot 10^{-3}$	$MgCl_2$ – SS1	
	S4	$9 \cdot 10^{-4}$	$3 \cdot 10^{-4}$	$MgCl_2$ – SS2	
	S5	$9 \cdot 10^{-5}$	$3 \cdot 10^{-5}$	$MgCl_2$ – SS3	
$AlCl_3$	SS3	$9 \cdot 10^{-3}$	$1.5 \cdot 10^{-3}$	$AlCl_3$ – SS1	
	S4	$9 \cdot 10^{-4}$	$1.5 \cdot 10^{-4}$	$AlCl_3$ – SS2	
	S5	$9 \cdot 10^{-5}$	$1.5 \cdot 10^{-5}$	$AlCl_3$ – SS3	

SS1/2/3… Stock solution 1/2/3; S4/5… Solution 4/5

VII Results and Discussion

With regard to the comparison of the zeta potential analysis of different regenerated cellulose fibers (and various surface treatments), great importance was attached to a reproducible and consistent measurement performance. One data point usually corresponds to 3 – 4 measurements (or more) in the presence of an electrolyte with a certain ionic strength at a defined pH value. With a measuring time per point of approx. 5 to 10 min it is assumed that temperature effects can be neglected. However, the influence of temperature is significant at very low ionic strengths, as the conductivity depends on the temperature, so it was considered that all measurements were performed at constant room temperature (25 °C).

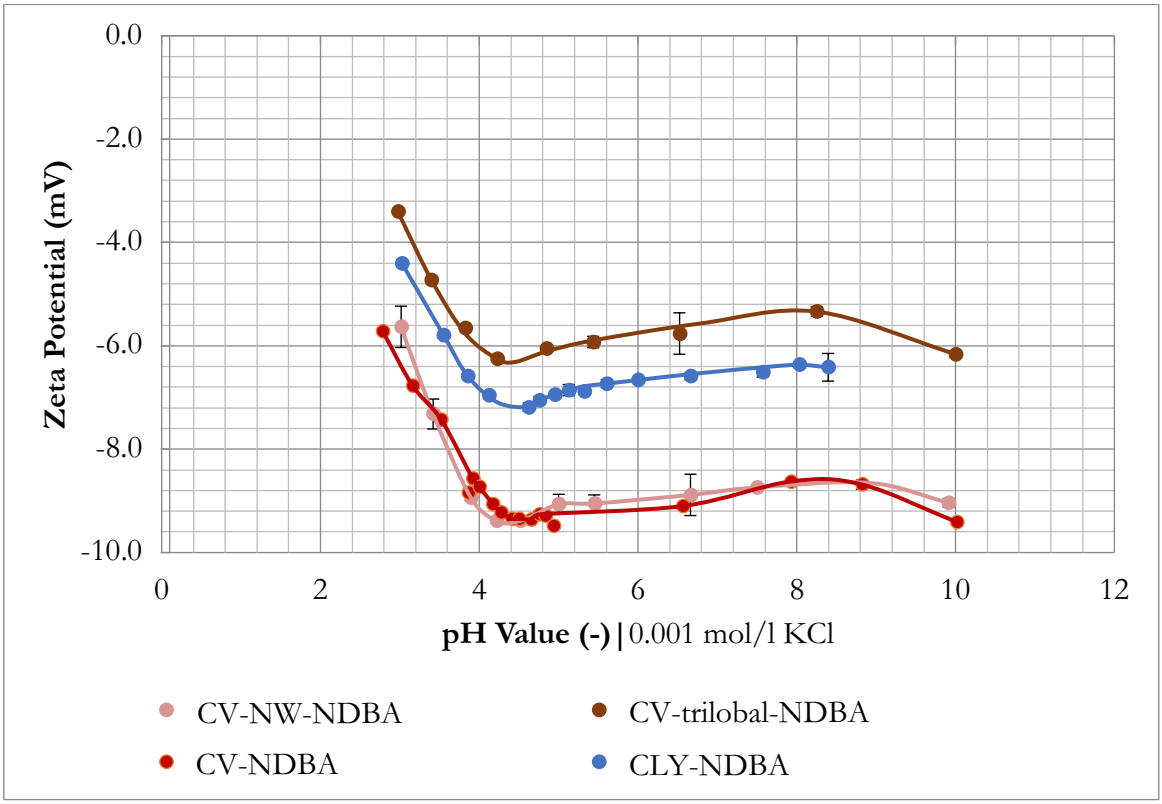

Fig. VII.I pH dependence (0.001 mol/l KCl) of zeta potential for three different types of viscose: Standard (CV-NDBA), red curve; nonwoven application (CV-NW-NDBA), rose curve; LENZINGViscostar® [9] (CV-trilobal-NDBA), brown curve; and Lyocell standard fiber (CLY-NDBA), blue curve.

[9] LENZINGViscostar® is a trademark of Lenzing AG

Regarding the zeta potential analysis of three different types of viscose fibers in comparison of Lyocell standard fiber CLY-NDBA (Fig. VII.I), clear differences can be observed between both viscose standard fiber (CV-NDBA) compared to Lyocell standard fiber and LENZINGViscostar® (CV-trilobal-NDBA) compared to CV-NW-NDBA and CV-NDBA. The measurements were performed as a function of pH value in the presence of a 0.001 mol/l KCl electrolyte solution. Disregarding the different bleaching process, LENZINGViscostar® fiber differs from the other viscose fibers investigated by its trilobal cross-section. In comparison, the values of the zeta potential for the trilobal viscose fiber are shifted parallel upwards (+3 mV). Because of its characteristic cross section, the LENZINGViscostar® fiber has evidently a much higher surface area and the packing in the fiber plug will be different, i.e. when absorbing water (or aqueous electrolyte solution), the special trilobal shape generates peculiar spaces between the fibers, thus improving the capillary effect. This effect is consistent with the dependence of the zeta potential on the fiber swelling and its adsorption characteristics.

The results in comparison to standard lyocell and viscose fibers differ from previous data in the literature [10]: The magnitudes of the negative zeta potential for viscose fibers were reported smaller in comparison to Lyocell, which is the opposite of the observation in Fig. VII.I. In relation to the results, how far do structural effects, (e.g., roughness) have influence on the magnitude of the zeta potential, the answer to this question has not yet been clarified. In principle, the streaming potential describes a macroscopic effect, but the charge contributions of the fiber, which are represented by the streaming potential, are microscopic or even nanoscopic (e.g., boundary layer). Further investigations with regard to differences in structural properties of both Lyocell and viscose fibers are necessary to discuss these results in more detail. However, the identical results for CV-NDBA (T_t = 1.3) and CV-NW-NDBA (T_t = 1.7) suggest that there is no dependence of the zeta potential with respect to the linear density of the fiber (titer).

VII.I Adsorption of Multivalent Ions

VII.I.I (1:1) Electrolyte – KCl

The dependence of the zeta potential for Lyocell and viscose standard fibers was investigated as a function of the conductivity (Fig. VII.II) or ionic strength (Fig. VII.III) of an aqueous KCl solution (1:1 electrolyte). In general, the course of the curve is to be expected for the complex sample (fiber sample) and cannot be explained by the classic model of the EDL.

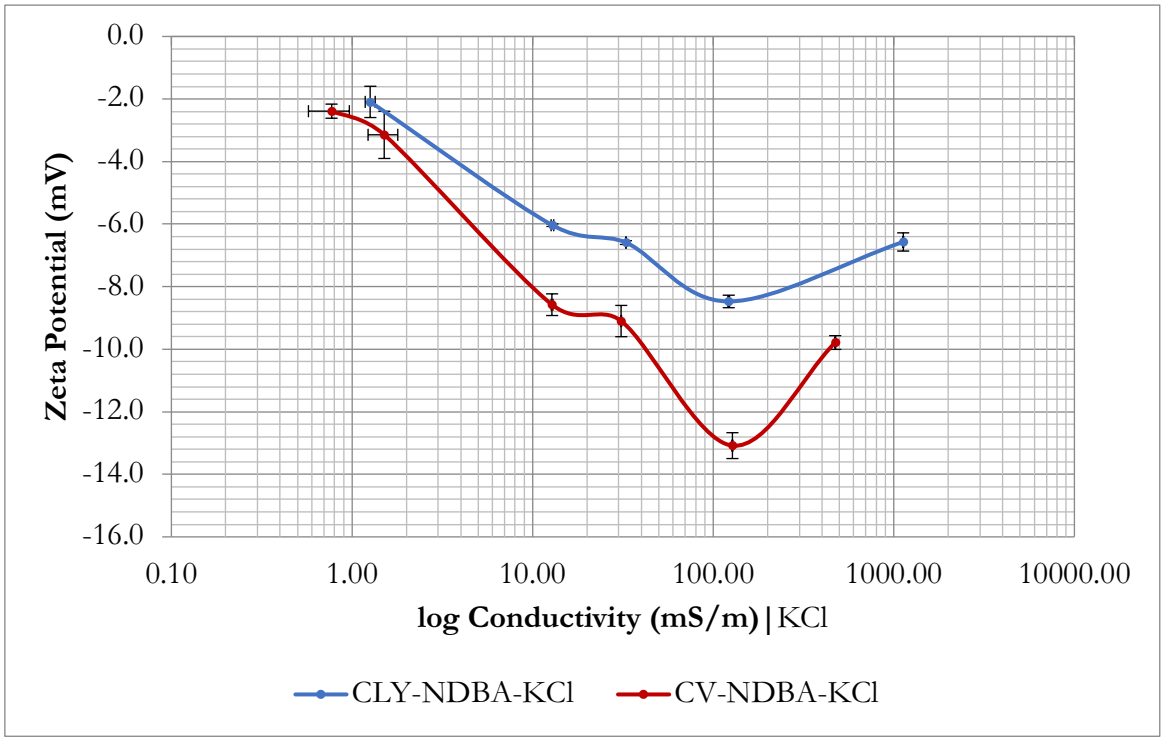

Fig. VII.II Dependence of the zeta potential of regenerated cellulose fibers (Lyocell and viscose; standard) on the conductivity of an aqueous KCl solution.

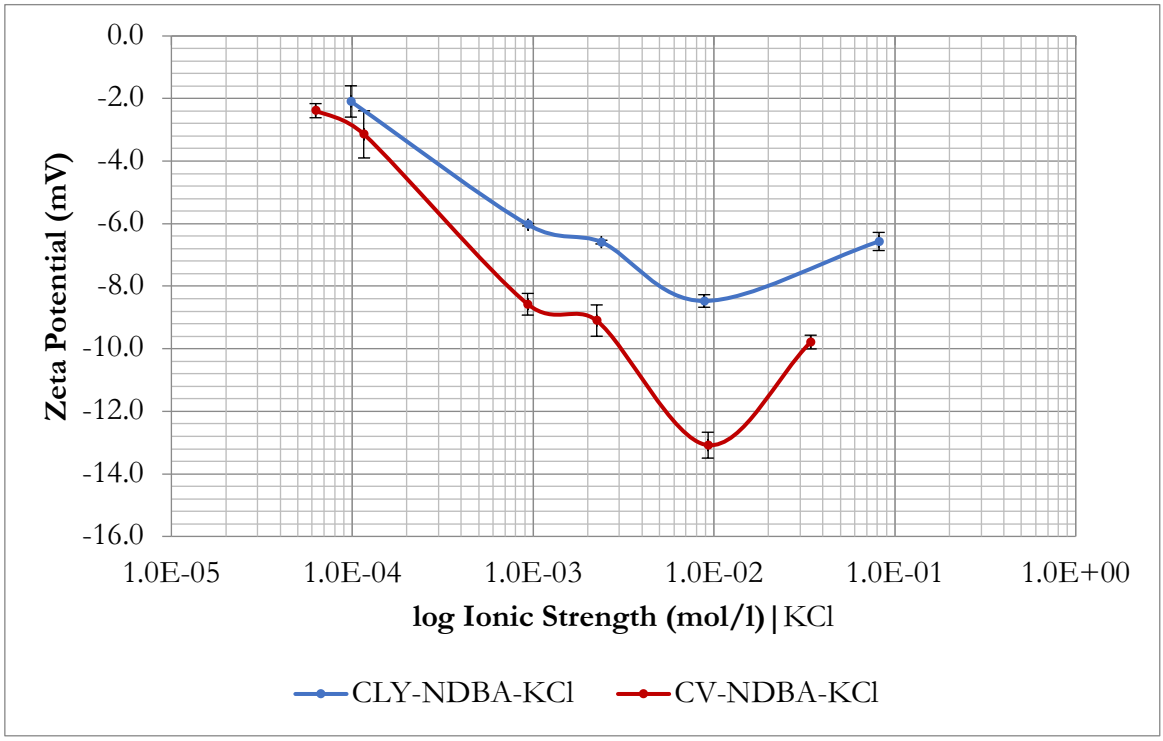

Fig. VII.III Dependence of the zeta potential of regenerated cellulose fibers (Lyocell and viscose; standard) on the ionic strength of an aqueous KCl solution.

According to the classic model of the EDL, a continuous decrease in magnitude of the zeta potential would be expected with increasing conductivity, which is the opposite of what can be observed. A decrease in the amount of the zeta potential only occurs at a conductivity of 125 mS/m or at an ionic strength of 0.009 mol/l, i.e., from 0.009 to 0.08 mol/l is a course that goes from theory to expectation. The results below an ionic strength of 0.009 mol/l (corresponding to 125 mS/m) are to be interpreted as apparent zeta potential, because especially at low ion strengths the data do not represent the real zeta potential values.

Both the slope of the curves and the position of the minimum are material properties or properties of the packing density. For comparable measurements, therefore, the reproducibility of the packing density (fiber plug) must be ensured, using the same fiber quantity for each measurement. The uniformity of the fiber packing density is represented by the permeability during the measurement. Therefore, a constant (recommended) permeability index of 100 was maintained during the measurements. Since the minimum as well as the curve progression for both viscose and Lyocell does not differ from the position with respect to the x-axis and the sample preparation, and the measurement procedure were performed according to the instructions, it can be assumed that the packing density was reproducible.

The course of the curve is therefore mainly related to the material properties, e.g. surface charge, swelling behavior, and porosity (if present). However, the minimum of the curve is comparatively localized at very high ionic strength (0.009 mol/l), but it should be noted that a significant localization of the minimum would require additional measuring points at different ion strengths. Additional measurements at closer ionic strength intervals could also provide more information about the formation of the peak in the curve at approx. 30 mS/m.

The characteristic curve is due in part to the swelling of the fiber. The swelling causes the fiber to become electrically conductive when in contact with water or an aqueous electrolyte solution. As mentioned before, this intrinsic conductivity of the fiber in the swollen state cannot be taken into account in the calculation of the zeta potential because it is not known. If the bulk electrolyte conductivity is very small compared to the unknown total conductivity, this results in significant miscalculation of the zeta potential, which obviously is the case at low ionic strength. (As mentioned in chapter V, according to the Helmholtz-Smoluchowski equation [Eq. (V.I)], the calculation of the zeta potentials is referred to the bulk electrolyte conductivity).

The reason for this error is not based on the measured streaming potential but the value of the electrical conductivity used for the calculation of the zeta potential. At high ionic strength, the conductivity of the electrolyte solution actually becomes representative of the total conductivity of the sample. Therefore, in case of KCl electrolyte solution, the values at high ionic strength (> 0.1 mol/l) are considered as real zeta potential values. The recorded values below 0.1 mol/l represent apparent zeta potential values, which indicates that the magnitude of the individual electrolyte conductivity is underestimated in the calculation.

After the mentioned impact of the packing density of the fibers on the zeta potential analysis, it is obvious that the distance between the randomly arranged fibers is of some importance, although the distance between the fibers is an effective size, i.e., some fibers are very close packed together in the fiber plug with including voids or cavities (otherwise it would not be possible for the liquid to flow through). Due to the fact that the fibers are on average very close to each other, the effective distance between the fibers does not correspond to the conditions for the applicability of the Helmholtz-Smoluchowski equation [Eq. (V.I)], and is therefore not appropriate for a correct calculation of the zeta potential [139].

According to the model of the EDL, an excess of counterions are present at the interface between the stationary layer and the diffusive layer and therefore a higher conductivity occurs compared to the bulk electrolyte. Since the cellulose fibers are very close to each other during the measurement, hence the ion concentration inside the pore channels between the fibers is higher compared to the liquid phase, i.e. the effect of the interfacial conductivity increases with decreasing distance between the fibers in the plug. Referring to a fiber system with no material swelling, the small distance between the fibers would cause the streaming potential to experience a higher conductivity not corresponding to the conductivity of the bulk electrolyte solution used for the calculation. Depending on the ionic strength of the electrolyte solution, this causes a certain expansion of the interfacial layer, which varies from, e.g., 1 nm for 0.1 molar KCl solution (Fig. VI.IV) to 100 nm for (ultrapure) water [122]. In consequence, the interfacial layer is further extended at low ionic strengths.

The representation of the calculated zeta potential as a function of the ionic strength proves to be more advantageous than the representation as a function of the conductivity, since the ionic strength is an absolute quantity and independent of the composition of the electrolyte. Conductivity, on the other hand, is a dependent variable, since the different mobility of separate ion species is a decisive factor and so is the concentration. This is intended for the

further representation of the measurements results. In addition, in the model of the EDL, the Debye length indicates the extension of the double layer and is represented as a function of the ionic strength. Fig. VI.IV compares the zeta potential as a function of the ionic strength of an aqueous KCl solution for standard Lyocell fiber with the compression of the electrochemical double layer with increasing electrolyte concentration (to be observed by a decay of the Debye length). The values were calculated using Eq. (V.V).

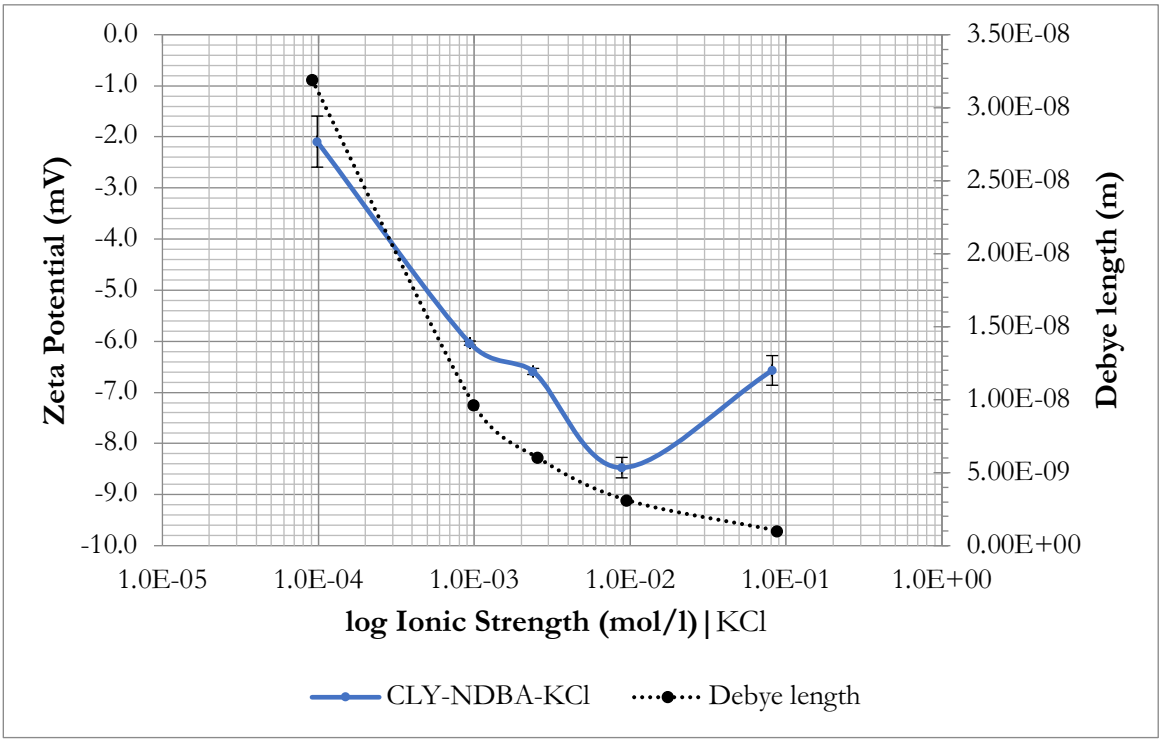

Fig. VII.IV Dependence of the zeta potential of Lyocell (standard) on the ionic strength of an aqueous KCl solution in comparison with the decay of the Debye length, indicating the extension of the EDL in correlation with the fiber spacing.

In oder to eliminate the effect of the interfacial conductivity, a different measurement setup should be considered, where the fibers can be arranged further apart (several micrometers) and thus, the expansion of the boundary layer is significantly smaller compared to the distance between the fibers. However, this required setup is not given by the principle of the measuring cell geometry with the respective fiber arrangement (fiber plug), moreover, at large fiber distances the prerequisite for the measurability of the streaming potential is not given, because the permeability of the sample would be much too high.

Another option regarding the elimination of the interfacial conductivity, is to increase the ionic strength of the solution. This means that even with small distances between the fibers, the interfacial layers of adjacent fibers do not tend to approach each other. In the presence of a KCl electrolyte solution, this effect can be observed experimentally above an ion strength of about 0.01, corresponding to a conductivity of about 125 mS/m, both for Lyocell and viscose fibers. The position of the minimum at about 0.009 mol/l (or 100 mS/m) is therefore to be interpreted as a property of the packing density.

However, the different slope of the individual curves for Lyocell and viscose is a material property. The differences in the properties of the two fibers Lyocell and viscose are therefore characterized by a different magnitude of the zeta potential at the minimum, i.e. the magnitude of the zeta potential at the minimum is attributed to a material property, but the corresponding ionic strength or conductance is basically a property of the packing density (fiber plug) and the material swelling.

It was suggested to implement a mathematical correction for the influence of the interfacial conductivity with regard to the zeta potential analysis of Lyocell and viscose fibers at different KCl electrolyte concentrations. This correction was first proposed by Fairbrother and Mastin in 1924 [130], according to which the quantity of the interfacial conductivity is determined by means of static resistance measurement. When performing the correction calculation according to Eq. (V.IV), it should be observed that the magnitude for the zeta potential increases, especially at lower ionic strengths but the results do not represent a significant deviation between the correct and the apparent zeta potential as shown in Fig. VII.V.

The application of the Fairbrother and Mastin method shows little difference compared to the measurements performed with SurPASS™ 3 according to Eq. (V.I.). Even at low ionic strength the resistance is comparatively very low due to the fiber packing density and the fiber properties. The instrument is not specified as a resistance analyzer and therefore the error is very large and cannot be measured with enough accuracy.

The Fairbrother and Mastin correction is intended to correct the influence of the interfacial conductivity and it applies to a rigid interface between solid and liquid phase, which is not to be expected with regenerated cellulose fibers. In particular, the swelling behavior results in a continuous transition between the fiber material and the liquid phase and not in a rigid

interface. Therefore, the swelling of cellulose fibers has a much greater effect on the magnitude of the zeta potential compared to the interfacial conductivity. Experience proves that the influence of the interfacial conductivity eliminates at an ionic strength above 10^{-3} mol/l. However, the results show that the minimum zeta potential is located at around 10^{-2} mol/l mentioned before, i.e., a further effect which is dominated by the material swelling of the fiber system.

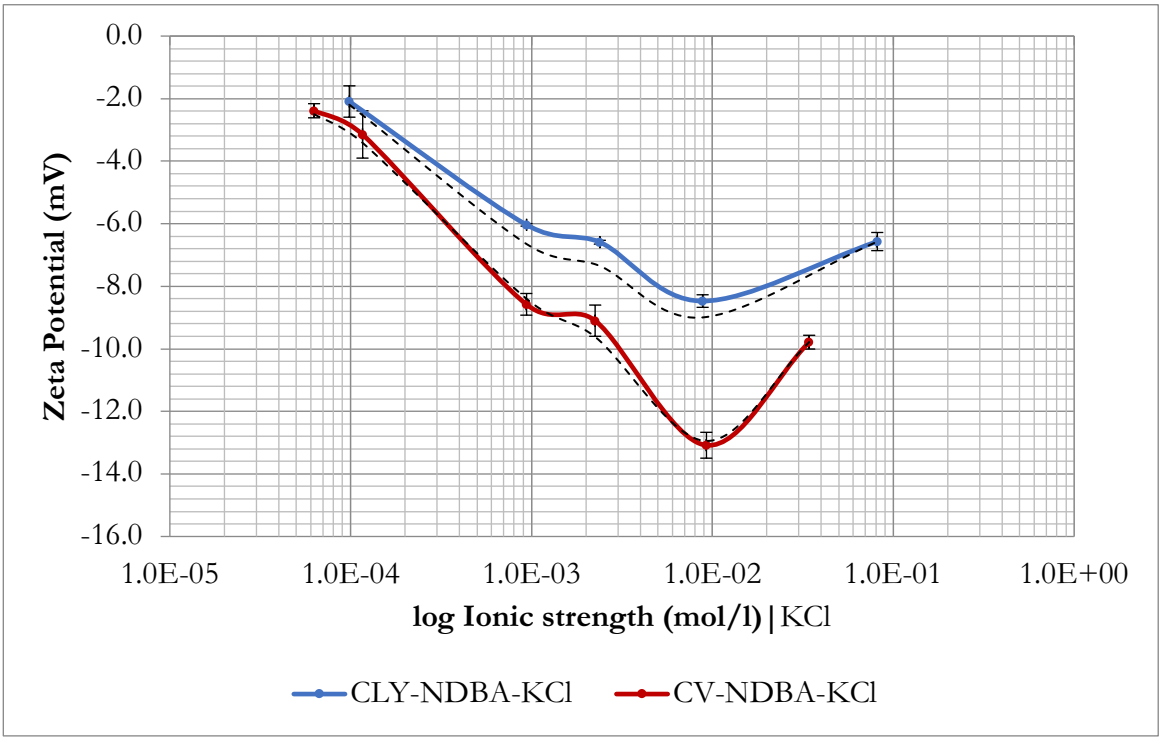

Fig. VII.V The zeta potential data for standard Lyocell and viscose evaluated from Eq. (V.IV), (correct; black broken line) compared to the apparent measurement results according to Eq. (V.I.).

Thus, it is proven that the Fairbrother and Mastin approach is not applicable to regenerated cellulose fibers and, as suspected in advance, the real zeta potential is not accessible at low ionic strength. Therefore, only an apparent zeta potential can be assumed for low ionic strengths. The fact that the Fairbrother and Mastin correction cannot be applied to regenerated cellulose fibers has not yet been discussed in the literature, but it is only of minor importance to the application to compare viscose and Lyocell fibers. For this reason, it is not recommended to apply this correction to the system of regenerated cellulose fibers.

VII.I.II (2:1) Electrolyte – $CaCl_2$ and $MgCl_2$

The dependence of the zeta potential for Lyocell and viscose standard fibers is represented as a function of ionic strength (Fig. VII.VI) of an aqueous $CaCl_2$ solution (2:1 electrolyte). Additionally, for CV-NDBA (standard viscose) the zeta potential at different ionic strength of $MgCl_2$ was investigated.

As already discussed in detail for the results as a function of KCl, the observed curve is characteristic for the complex fiber sample. Therefore, the conclusions regarding the effects of the characteristic properties of cellulosic fibers on the zeta potential analysis (e.g. swelling, fiber packing density, extension of the EDL) are also valid for the discussion of the results concerning complex electrolytes.

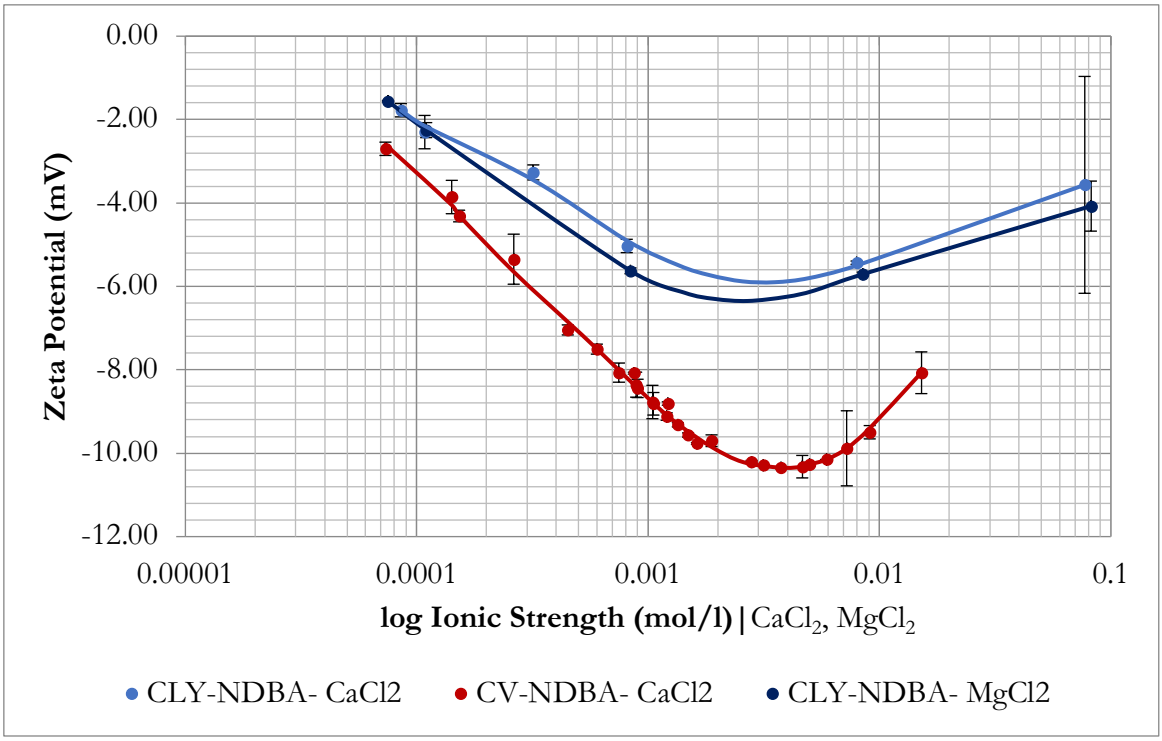

Fig. VII.VI Dependence of the zeta potential of regenerated cellulose fibers (Lyocell and viscose; standard) on the ionic strength of an aqueous $CaCl_2$ (and $MgCl_2$) solution.

In the results for viscose with divalent Ca^{2+} ions, the positive effect on the characteristic of the curve becomes clear when the measurements are performed by the stepwise addition of concentrated electrolyte solution. Due to the higher density of measurement points it can be seen that the curve is indeed almost linear on the left side of the minimum. The minimum for CV-NDBA-$CaCl_2$ is located at 0.004 mol/l and shifted to lower ionic strength compared

to the results for KCl (0.009 mol/l). The same shift to low ionic strengths is observed for standard Lyocell fibers, both in the presence of $CaCl_2$ and $MgCl_2$. Moreover, the magnitude of zeta potential is comparatively lower (-10.35 mV, CV-NDBA-$CaCl_2$; -13.10 mV, CV-NDBA-KCl; -5.80 mV, CLY-NDBA-$CaCl_2$; -8.50 mV, CLY-NDBA-KCl).

The error bars are particularly noticeable for Lyocell in the higher ionic strength range but have no negative impact on the interpretation of the data.

According to expectations, the results show that the bivalent ions (Ca^{2+}, Mg^{2+}) are involved in the formation of the zeta potential for both Lyocell and viscose fibers, i.e. the ions have been adsorbed on the fiber surface at a certain amount and thus have an effect on the magnitude of the zeta potential. A specific interaction of the fiber in comparison of calcium and magnesium ions is not clearly recognizable from the measured data. Therefore, no higher affinity of the Lyocell fiber to Ca^{2+} ions compared to Mg^{2+} ions can be assumed.

Despite of the fact that the resulting magnitude of the zeta potential for Lyocell and viscose are comparatively small, the two curves differ significantly, even if the minima of the two fiber types differ only by about 5 mV (in accordance with the results for KCl). The results indicate that the material differences between the two regenerated cellulose fibers are reflected in the zeta potential analysis. One reason for the material differences between Lyocell and viscose is the different manufacturing process of the two regenerated cellulose fibers. In the viscose process, cellulose is converted into cellulose xanthate (derivatization) and thus becomes soluble (chemical process). The production of Lyocell fibers is a physical process, where the cellulose is dissolved directly in an organic solvent (NMMO) without chemical modification. As a result of the differences in the spinning process, the respective characteristic morphology of the two fibers is formed. Lyocell fibers exhibit a smooth surface (round cross-section), whereas viscose fibers show longitudinal indentations (irregular cross-section). Therefore, the specific surface area of viscose fibers is higher than that of Lyocell fibers.

VII.I.II (3:1) Electrolyte – $AlCl_3$

The measurement results for standard Lyocell and viscose fibers with different ionic strength of $AlCl_3$ show further interesting observations (Fig. VII.VI). However, a shift of the minimum to again lower ionic strength in comparison to the measurements with divalent cations is observed in the graphic (-6.80 mV, CV-NDBA-$AlCl_3$; -8.30 mV, CLY-NDBA-

$AlCl_3$). Nevertheless, the magnitude of the zeta potential for Lyocell is comparatively higher than for viscose, (i.e., in Fig. VII.VII the blue curve is seen below the red curve), which is an opposite observation compared to the previous measurements in the presence of mono- and bivalent ions (KCl, $CaCl_2$).

The characteristic of the curves again indicates the swelling of the fibers but differs in its curvature compared to KCl, $CaCl_2$ and $MgCl_2$. While the graph for the viscose fiber initially follows the criteria for negative curvature, the graph for the Lyocell fiber shows a positive curvature. For the last two measuring points the Lyocell fiber reaches a plateau and converges to the x-axis, i.e. the zeta potential approaches a steady-state value which is close to zero. Despite the comparatively high ionic strength, the error bars are low.

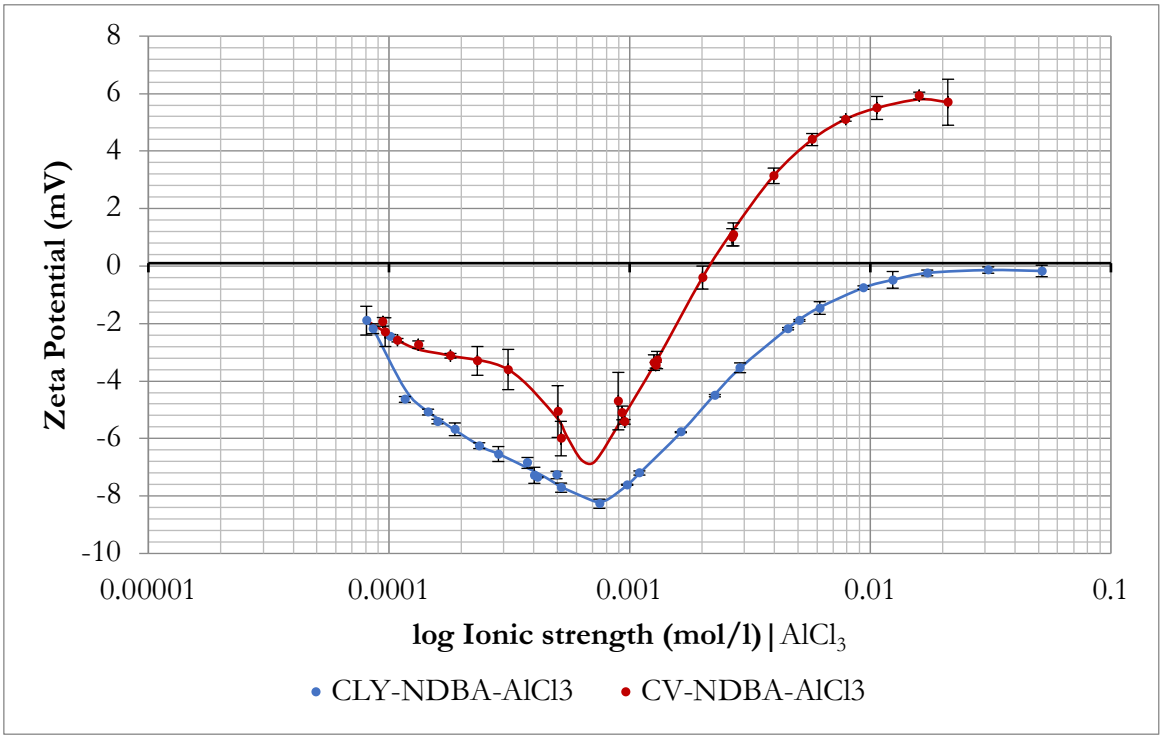

Fig. VII.VII Dependence of the zeta potential of regenerated cellulose fibers (Lyocell and viscose; standard) on the ionic strength of an aqueous $AgCl_3$ solution.

The reason for the formation of the plateau is that no further ions can be adsorbed into the interfacial layer. Although the viscose fiber has a higher specific surface area, the negatively charged surface in aqueous solution becomes positive as the ion concentration is raised above 0.002 mol/l, whereas the curve for the Lyocell fiber remains below the x-axis. This characteristic of the curve confirms the higher affinity of the viscose fiber to Al^{3+} ions. However, the question arises regarding the possible explanation for the higher affinity of

Al^{3+} ions for viscose compared to Lyocell fibers. Considering the extreme curve progression of the viscose fiber at high ionic strength, it can be assumed that the effect is not only caused by a physical adsorption but the Al^{3+} ions also tend to form complexes or interact chemically with the fiber surface. $AgCl_3$ itself has a very pronounced affinity for water (hygroscopic properties) and when mixed with water, the Cl^- ions get replaced with water molecules in the lattice to form the hexahydrate ($Al(H_2O)_6Cl_3$) and partially dissociates in aluminum hydroxide and HCl, depending on the pH of the solution (hydrolysis) [140].

Similar results were obtained by Mosur et al. [141] for their investigation of the pH dependences of the zeta potential of MCC (microcrystalline cellulose) particles in aluminum chloride solution with different concentrations. Further Baty et al. [142] reported, however, an important mechanism of degradation in papermaking in the presence of Al^{3+} (the metal cation in alum).

VII.II Hydrophobic Lyocell and Viscose Fibers

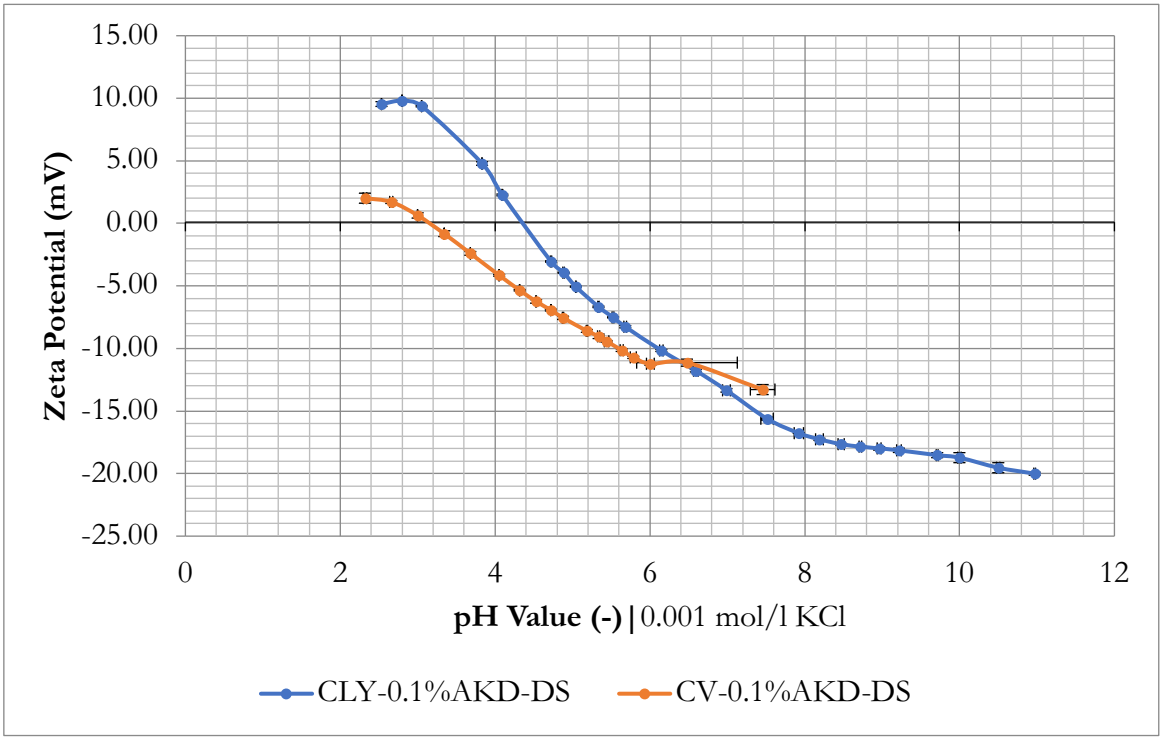

Fig. VII.VIII pH dependence of the zeta potential of hydrophobic (0.1% AKD) regenerated cellulose fibers (Lyocell and viscose; standard) in the presence of 0.001 mol/l KCl electrolyte solution.

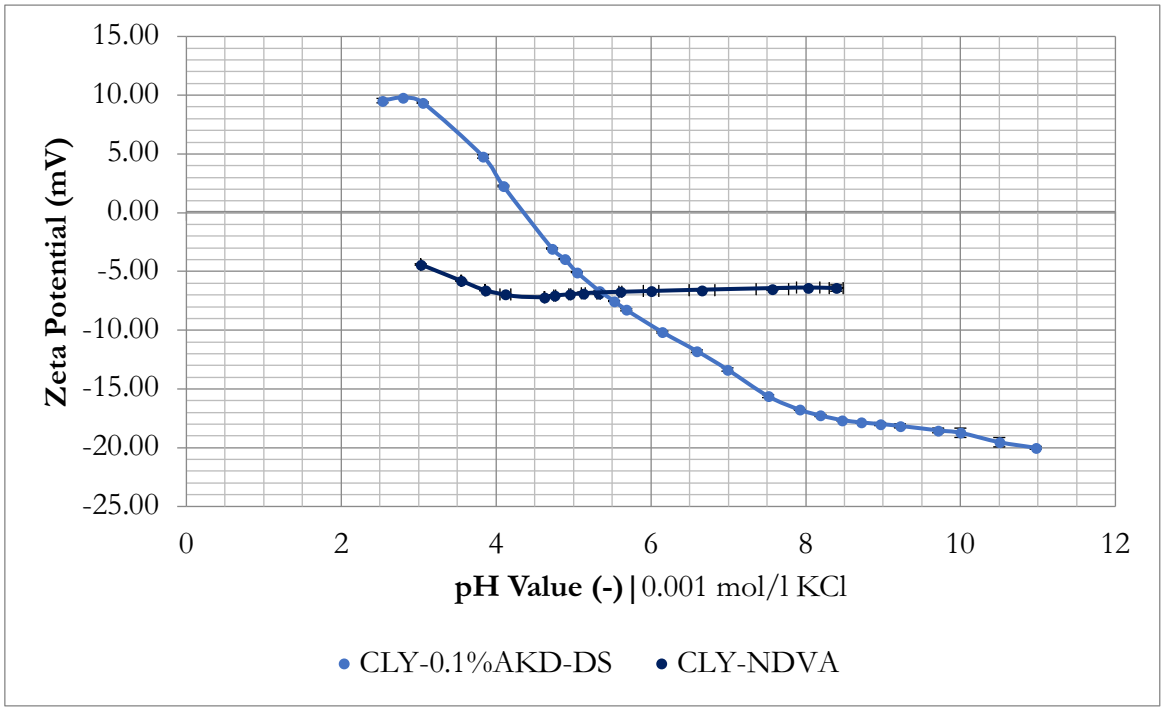

Fig. VII.IX pH dependence of the zeta potential in comparison of hydrophobic and untreated Lyocell fibers in the presence of 0.001 mol/l KCl electrolyte solution.

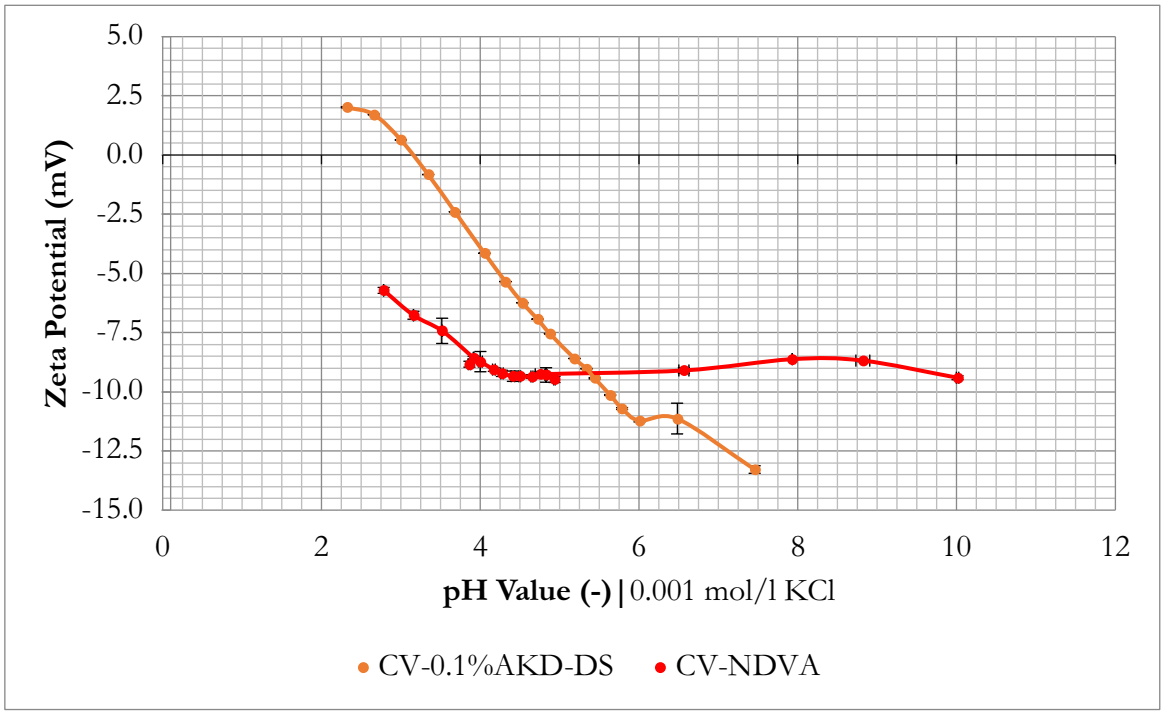

Fig. VII.X pH dependence of the zeta potential in comparison of hydrophobic and untreated viscose fibers in the presence of 0.001 mol/l KCl electrolyte solution.

Details about the AKD-modification of cellulose fibers are discussed in the literature [143–145] and should be further mentioned there. For the discussion of the results it should be sufficient that this treatment is used for the hydrophobization of cellulose fibers.

For regenerated cellulose fibers treated with AKD (alkyl ketene dimer), differences between Lyocell and viscose are also observed (Fig. VII.VIII). The graphic represents the measurement results as a function of the pH value in the presence of 10^{-3} mol/l KCl electrolyte solution. If the results for CLY-0.1%AKD-DS are compared with the untreated fiber (Fig. VII.IX), no increase in the curve can be observed in the alkaline range. At high pH values, the magnitude of zeta potential of the fiber treated with AKD is more negative compared to the untreated fiber, for both Lyocell and viscose (Fig. VII.IX and Fig. VII.X).

With regard to an entirely hydrophobic fiber, an isoelectric point (IEP) at pH 4 would be expected, i.e. as a characteristic of material surfaces that have no functional groups. This phenomenon is a consequence of the adsorption equilibrium of water ions on hydrophobic surfaces, which is reached at pH 4. Hydroxide ions (OH^-) and hydronium ions (H_3O^+) differ in their physiochemical properties in terms of size, polarizability and also in their attraction to water molecules, i.e. hydrate shell, which should keep the two ions separate. As a result of these different properties, the hydroxide ions exhibit a higher level of affinity to hydrophobic surfaces than the hydronium ions. Therefore, H_3O^+ concentration in the aqueous solution must exceed that of OH^- to achieve an equivalent adsorption of the two ions at hydrophobic interfaces, i.e., it takes 1000 times more H_3O^+ ions to adsorb in the same number of OH^- ions on the hydrophobic surface and is intended to be sufficient as a qualitative explanation.

Nevertheless, the hydrophobic property of the AKD Lyocell fiber is more pronounced as compared to AKD treated viscose fiber. For AKD Lyocell it can be seen that a curve plateau is reached at low pH values, which is also lightly marked for AKD viscose. In the course of the AKD Lyocell curve a small maximum is reached at +10 mV (at pH = 2.8).

This trend reversal at low pH values results from the high ionic strength of the aqueous solution due to the added acid (HCl), taking into account the higher activity of hydronium ions (H_3O^+) compared to K+ ions. The observed pH effect on the zeta potential is determined by the increase of ionic strength with decreasing pH value and therefore a valid evaluation of the data at low pH values is difficult. An exception to this is observed at high pH values where there is no effect on the zeta potential with regard to increasing ionic

strength (or conductivity) of the bulk electrolyte solution, and therefore, the recorded data in the range of pH 4–10 can be interpreted based on the pH dependence of the zeta potential. This information is valid for the use of a 10^{-3} mol/l KCl solution.
At low pH values it is therefore critical to state that the magnitude of the zeta potential increases with lower pH values, because the effect of the higher ionic strength is observed simultaneously.

The graphic (Fig. VII.VIII) shows another interesting example of the difference between the two regenerated cellulose fibers. The two fibers also show different results for the AKD treatment, as already noted for the adsorption of multivalent ions. The comparison between the zeta potential data for the AKD Lyocell and viscose fibers indicates a preferential bonding of the AKD to the Lyocell fiber.

The AKD-treated regenerated cellulose fibers show clear hydrophobic properties based on the zeta potential data, especially when comparing the data with the untreated fibers (Fig. VII.IX and Fig. VII.X), which would also result from the determination of the contact angle but are difficult to investigate for fibers.

Since Lyocell and viscose fibers have already been treated with AKD (and the hydrophobing agent has not been applied in the measurement, e.g., $AlCl_3$ adsorption), the measurement results also indicate the stability of the AKD treatment. If the AKD treatment had washed out, neither an IEP close to 4 nor the very negative zeta potential in the alkaline range would be observable, but due to contact with the aqueous solution it cannot be excluded that the hydrophobic effect has been washed away

With regard to the AKD treated viscose fiber, it can be assumed that the ADK treatment is either less effective, i.e. leads to a less hydrophobic character or the exposure to the aqueous solution tends to an effective reduction of the hydrophobic property. Further investigations are necessary to confirm the assumptions, e.g. storing the fibers in water for a longer period of time.

Based on this approach, the zeta potential measurements are applicable for quality control during the manufacturing process of hydrophobic fibers.

VII.III Cationic Viscose Fibers

Due to the fact that this treatment of cellulose fibers is still in trial, no further details about the treatment can be specified. It should nevertheless be sufficient for the discussion that (in this case) viscose fibers treated by this method exhibit a positive surface charge in contact with an aqueous solution. In order to exclude possible effects of the avivage, the fiber sample without avivage (WA) was chosen for this measurement.

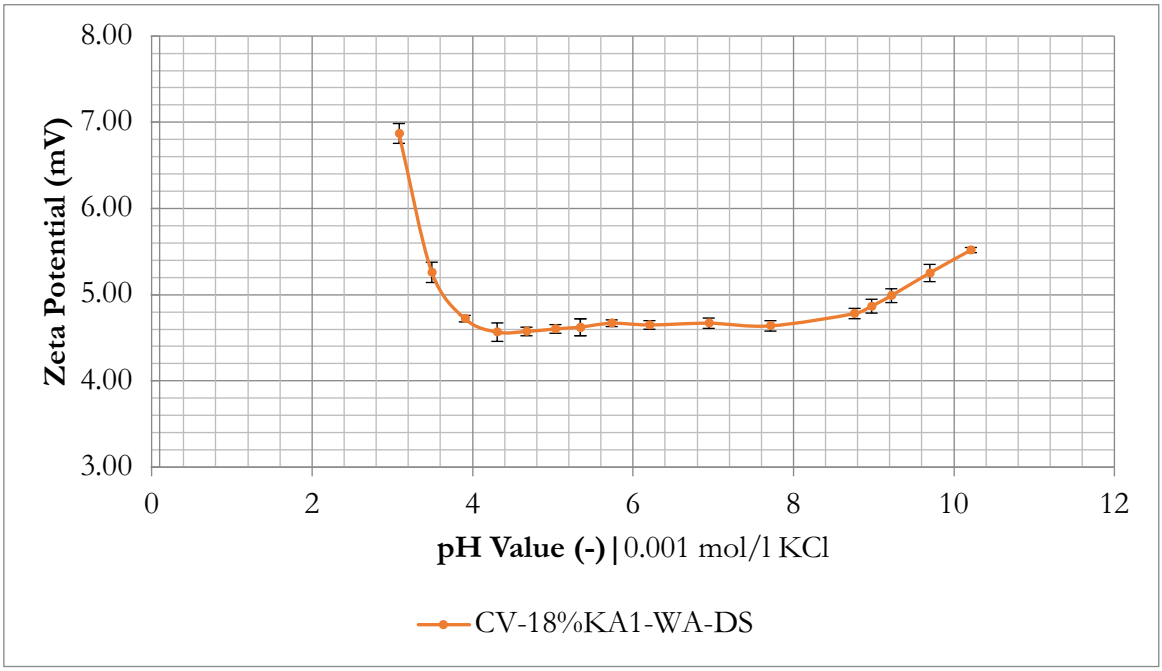

Fig. VII.XI pH dependence of the zeta potential of viscose fibers treated with a cationic additive (18% KA1) in the presence of 0.001 mol/l KCl electrolyte solution.

The results in Fig. VII.XI show the influence of the cationic modification, which causes a positive charge of the fiber surface over a wide pH range. Significantly, the sign of the zeta potential is positive, and the results show an expected course for viscose (resp. cellulose) fibers treated with a cationic additive (KA). The curve falls linearly, then reaches a plateau (pH 4) until it rises at pH 8. Due to the fact that the measurements were also performed in the presence of a 10^{-3} mol/l KCl solution, the already discussed limiting conditions for the pH dependence of the zeta potential also occur for this investigation, i.e., for the recorded data at pH < 4, the pH dependence of the zeta potential is impaired by the conductivity effect, especially at low pH values and is not to be interpreted as a characteristic of this cationic treatment. The same effect of conductivity applies to higher pH values (pH > 9), which means that the increase in zeta potential with increasing pH is equally affected by the higher conductivity of the electrolyte solution. In other words, the characteristics of the zeta potential as a function of the pH value is more an effect of the conductivity of the electrolyte

solution. This effect would be significantly lower when using a more concentrated electrolyte solution.

Nevertheless, the physicochemical and structural properties of the regenerated cellulose fibers affect the magnitude of the zeta potential, e.g., swelling, packing density (fiber plug), extension of the EDL. Therefore, it can be assumed that the alleged real zeta potential is shifted to higher values for these measurements as well; an intentional miscalculation that is (or must be) made due to the inaccessible conductivity in the fiber plug.

The interpretation of the measurement results leads to the conclusion that cationic modified viscose fibers are not affected by the pH of the electrolyte solution and retain the cationic properties over the entire pH range, i.e., the effect of the cationic additive is not changed by contact with the electrolyte solution.

It should be noted that most zeta potential measurements published in the literature are performed on inherent negatively charged surfaces and that there is comparatively little information about positively charged materials as a function of ionic strength.

VII.III.II Viscose Fibers with different amount of KA

With regard to differences in the zeta potential analysis of cationic viscose fibers, 5 samples with different percentage of cationic additive(s) were investigated. To prevent the results from possible influences of the water solubility of the avivage components during the measurement, an adapted measurement setup was used (mentioned in detail in chapter VI). It proved to be difficult to set the required permeability (PI = 100) for the measurement, as this can only be controlled by the amount of fiber filled into the measuring cell. However, since the zeta potential is dependent on the permeability of the fiber sample, different PI were adapted for this investigation.

The measurements were therefore performed with different amounts of viscose fiber (using a 0.001 mol/l KCl electrolyte solution) and plotted as a function of permeability (represented by the permeability index (PI)) and are illustrated in Fig. VII.XII. The error bars have been omitted for a more favorable presentation of the data. It was to be expected that with regard to higher additive concentration the zeta potential would shift to higher values, but this assumption can only be confirmed for CV-25%KA1-DS. A comparison of the corresponding zeta potential values (for similar PI) clearly shows that there is no significant

correlation between the quantities of additives and the magnitude of the zeta potential. However, it can be seen that the magnitude of the zeta potential decreases with decreasing permeability.

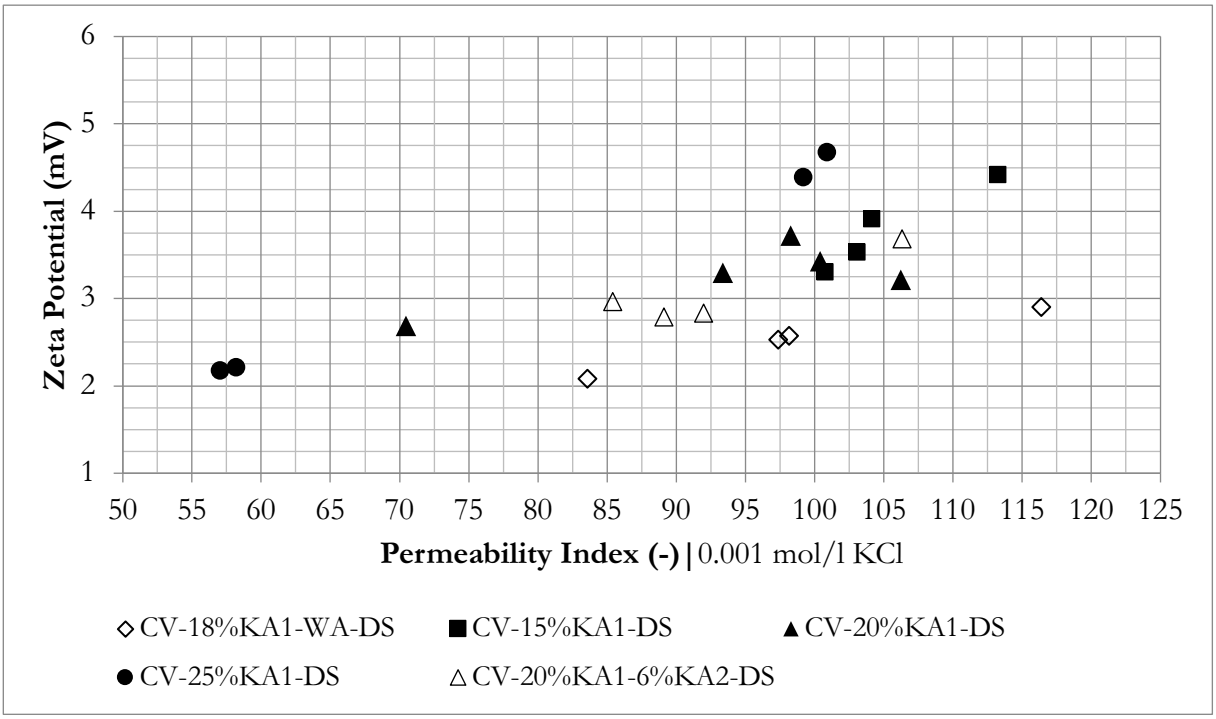

Fig. VII.XII Dependence of the zeta potential of viscose fibers with different percentage of cationic additive(s) on the permeability index in the presence of 0.001 mol/l KCl electrolyte solution.

VII.III.II The Effect of Avivage Treatment

As already mentioned, the possibility of washing off the components of the avivage when the fiber is immersed in an aqueous solution limits the applicability of the zeta potential analysis for regenerated cellulose fibers, i.e., the fibers to be examined need to be sampled before the avivage is applied in the manufacturing process. This limitation is nevertheless relevant for the investigation of cellulose fibers at the end of the production process.

Due to the fact that (except for one sample) the viscose fibers with different amounts of cationic additives were provided *with aviviage*, the possible influence on the zeta potential analysis was investigated for the sample CV-15%KA1-DS. The results (zeta potential and pH) are illustrated in Fig. VII.XIII as function of time. A more distinct illustration of the dependence of the zeta potential as a function of time is shown in Fig. VII.XIV.

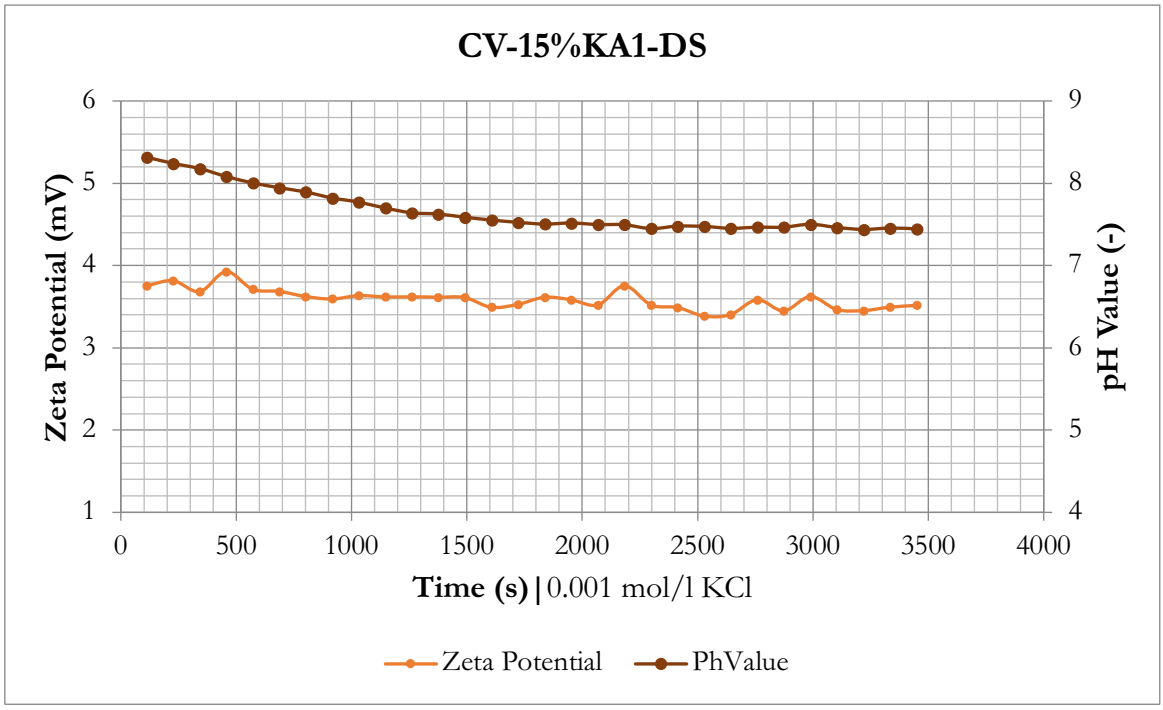

Fig. VII.XIII Time dependent zeta potential (and pH) of viscose fibers treated with a cationic additive (15% KA1) and avivage in the presence of 0.001 mol/l KCl electrolyte solution.

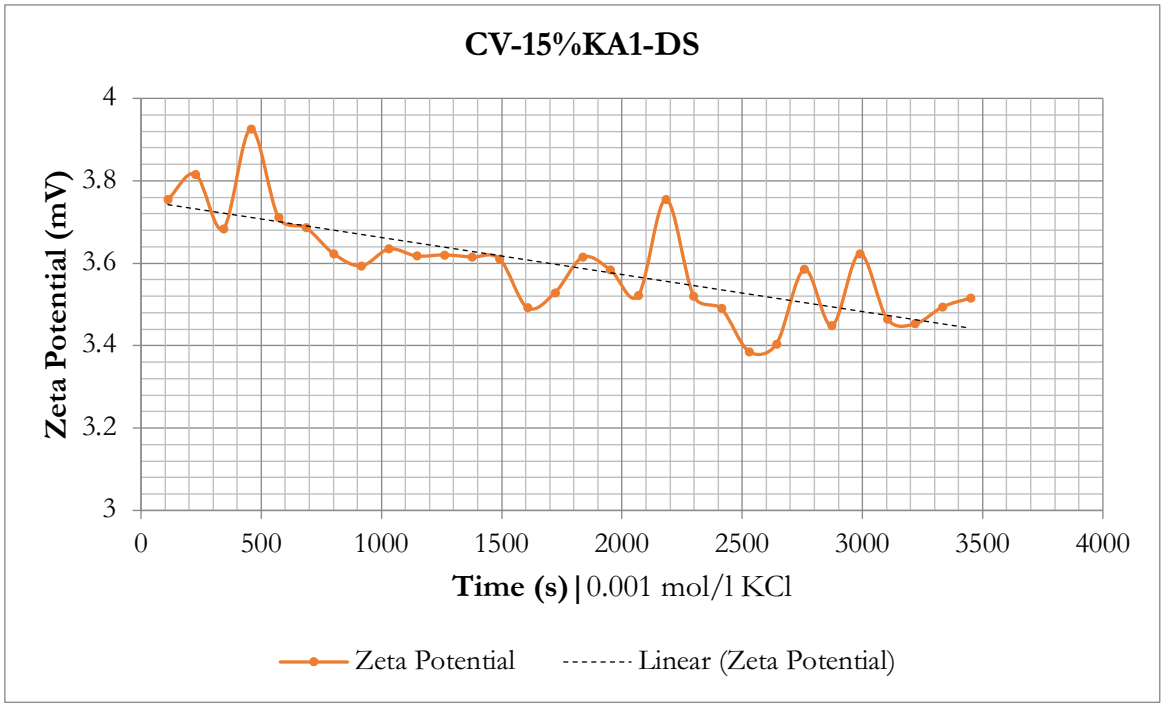

Fig. VII.XIV Time dependent zeta potential of viscose fibers treated with a cationic additive (15% KA1) and avivage in the presence of 0.001 mol/l KCl electrolyte solution, and linear regression (black broken line).

The effect on the zeta potential due to the solubility of the avivage is observed to be relatively small. The maximum deviation of the magnitude of the zeta potential is about ±0.25 mV. However, the change in the pH value (8.3 – 7.5) of the electrolyte solution during the measurement can be seen more clearly as the measuring time progresses. A comparison with the measurement in Fig. VII.XI indicates that the zeta potential is almost constant in the range of pH 4 to 8, and therefore this observed pH effect caused by the sample should not influence the course of the zeta potential. From this perspective, it is still ambiguous whether the change in pH is a cause of the avivage or the cationic additive, while different time dependency of the zeta potential can also give information about the swelling of the fibers in contact with an aqueous solution.

VII.IV Alkali cellulose

The results for the investigations on the system alkali cellulose as a function of the pH value (Fig. VII.XV) show high dispersions of values (i.e., comparatively large error bars). Therefore, the (possible) course of the curve has not been marked for this example. In the range of a pH of 4.5, a minimum of the zeta potential can be observed at approx. -7.3 mV.

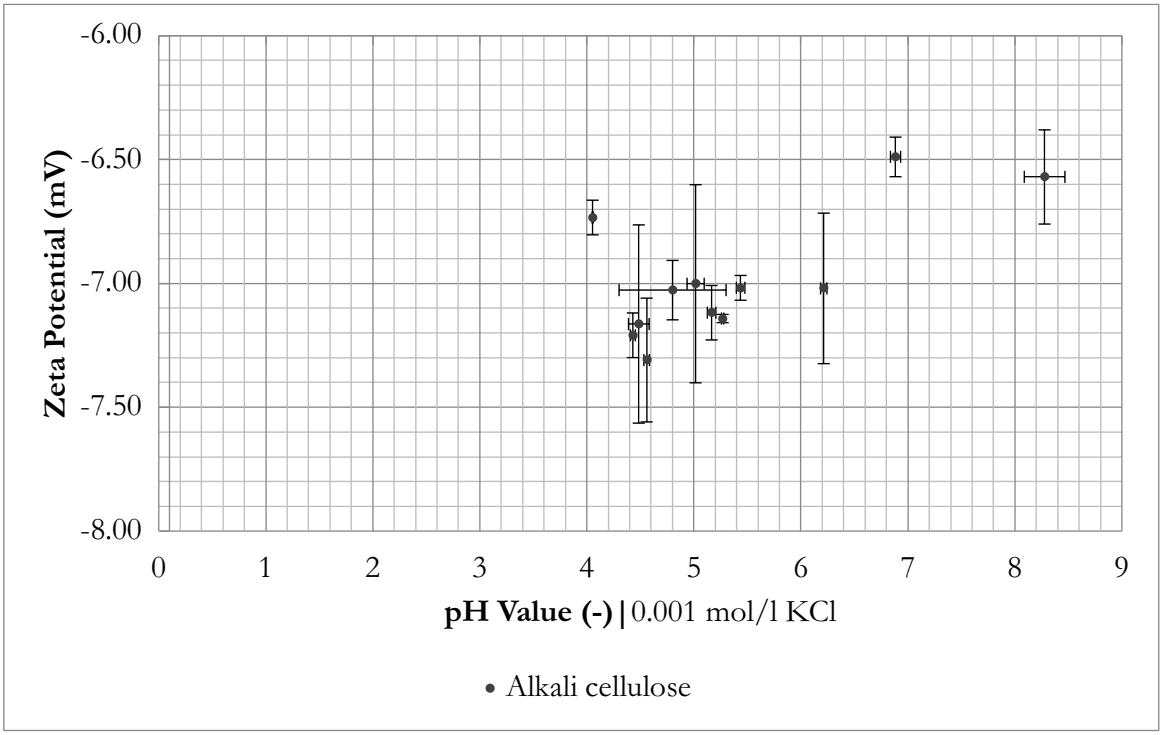

Fig. VII.XV pH dependence of the zeta potential of alkali cellulose in the presence of 0.001 mol/l KCl electrolyte solution.

Although the deviation range is comparatively large, the curve of a characteristic cellulosic material can be assumed. During the performance of the measurement, the assumption was confirmed that the sample had not been (or could not be) washed sufficiently neutrally after sampling from the manufacturing process by changes in the pH value of the electrolyte solution during the analysis and difficulties in the adjustment of low pH values. This effect of the residual alkali content of the sample is probably responsible for the high dispersion of the data.

As a consequence, the alkali cellulose is therefore less suitable for the zeta potential analysis, since a residual alkali content in the sample cannot be entirely eliminated.

VIII Conclusion

In this master's thesis a number of different regenerated cellulose fibers from Lenzing AG (Austria) were characterized by zeta potential measurements. Despite of the complex behavior of regenerated cellulose fibers, (e.g., interfibrillar porous structure, structural differences in the outer surface compared to bulk, high swelling propensity in aqueous solutions, and the restriction of the apparent zeta potential) the effect of distinct fiber treatments clearly becomes evident from electrokinetic measurements.

The comparison of measurement data of untreated (standard) Lyocell and viscose fibers showed significant differences, which were presumably linked to structural properties, but could not be directly explained by electrokinetic effects. Compared to conventional viscose fibers, the results for LENZINGViscostar® fibers with characteristic trilobal cross-section deviated to significantly lower values, regarding the order of magnitude of the negative zeta potential.

The results for different electrolytes and ionic strengths could not be explained with the classical model of EDL and were therefore to be interpreted as apparent zeta potential values. Especially the swelling behavior as a characteristic material property of cellulosic fibers is reflected in the zeta potential analysis. Furthermore, it could be shown that the Fairbrother and Mastin approach to correct the influence of the interfacial conductivity in the calculation of the zeta potential is not applicable to the complex system of cellulose fibers.

Concerning the measurement results for polyvalent ions, a significantly higher affinity of the lyocell fiber to Ca^{2+} or Mg^{2+} could not be confirmed. However, lower zeta potential values were registered both for the curve for Lyocell and for viscose fibers compared to monovalent ions (K^{+}). The measurement results for standard Lyocell and viscose fibers with different ionic strength of $AlCl_3$ could not be fully explained by the effect of physical adsorption and require further investigation with different analytical techniques (e.g., ICP-MS).

For regenerated cellulose fibers treated with AKD, differences between Lyocell and viscose could also be determined and the characteristic effect of hydrophobization was clearly visible in the measurement results. The treatment of viscose fibers with different amounts of cationic additive was found to be constant over a wide pH range, although a correlation between different percentage of cationic additive(s) could not be investigated with the considered measurement setup. In contrast to the expectations, the effect of the avivage on the zeta potential could be monitored relatively small. Nevertheless, possible effects of post-treatments, (e.g., avivage, refinements, or drying) should always be taken into account when performing zeta potential analysis of regenerated cellulose fibers.

Since there is only limited information about the zeta potential analysis of positively charged macroscopic solids in the literature so far, this cationic fiber treatment proves to be particularly interesting for further investigations from a scientific point of view.

The alkali cellulose proved to be rather unsuitable for the zeta potential analysis because of its strong alkaline properties.

Although the zeta potential analysis of cellulose fibers has its limitations, it can be used for the monitoring of fiber swelling and their absorption properties towards different multivalent ions as well as quality control for different fiber treatments. However, it should be noted that further measurements and investigations are essential in terms of reproducibility and the potential use as routine measurement equipment for surface charge analysis of regenerated cellulose fibers.

List of References

1 L. Fras, J. Laine, P. Stenius et al., *Determination of dissociable groups in natural and regenerated cellulose fibers by different titration methods*, J. Appl. Polym. Sci. 92(5) (2004) 3186–3195.

2 L. Fras-Zemljič, Z. Peršin, P. Stenius, K. Stana-Kleinschek, *Carbooxyl groups in pre-treated regenerated cellulose fibres*, Cellullose 15 (2008) 681.

3 V. Ribitsch, K. Stana-Kleinschek, T. Kreze, S. Strnad, *The significance of Surface Charge and Structure on the Accessibility of Cellulose Fibres*, Macromol. Mater. Eng. 286(10) (2001) 648–654.

4 K. Stana-Kleinschek, V. Ribitsch, T. Kreze, L. Fras, *Determination of the adsorption character of cellulose fibres using surface tension and surface charge*, Mater. Res. Innov. 6(1) (2002) 13–18.

5 F. Weber, G. Koller, R. Schennach et al., *The surface charge of regenerated cellulose fibres*, Cellulose 20 (2013) 2719–2729.

6 A. E. Horvath, T. Lindström. J. Laine, *On the Indirect Polyelectrolyte Titration of Cellulosic Fibers. Conditions for Charge Stoichiometry and Comparison with ESCA*, Langmuir 22(2) (2006) 824–830.

7 H. Zhang, C. Zhao, Z. Li, J. Li, *The fiber charge measurement depending on the poly-DADMAC accessibility to cellulose fibers*, Cellulose 23 (2016) 163–173.

8 R.I.S. Gill, *The use of potentiometric titration and polyelectrolyte titration to measure the surface charge of cellulose fibre*, in Fundamentals of Papermaking, Trans. of the 9th Fund. Res. Symp. Cambridge, 1989, (C.F. Baker, V. Punton, eds.), FRC, Manchester (UK), 2018, pp 437–452.

9 J. Lützenkirchen, T. Preočanin, D. Kovačević et al., *Potentiometric Titration as a Tool for Surface Charge Determination*, Croat. Chem. Acta 85(4) (2012) 391–417.

10 K. Stana-Kleinschek, T. Kreze, V. Ribitsch, S. Strnad, *Reactivity and electrokinetical properties of different types of regenerated cellulose fibres*, Colloids and Surfaces A: Physiochem. Eng. Aspects 195 (2001) 275–284.

11 M. Elimelech, W. H. Chen, J. J. Waypa, *Measuring the zeta (electrokinetic) potential of reverse osmosis membranes by a streaming potential analyzer*, Desalination 95(3) (1994) 269–286.

12 H.-J. Jacobasch, G. Bauböck, J. Schurz, *Problems and results of zeta-potential measurements on fibers*, Colloid Polymer Sci 263 (1985) 3-24.

13 M. Reischl, S. Köstler, G. Kellner et al., *Oscillating streaming potential measurement system for macroscopic surfaces*, Rev. Sci. Instrum. 79(11) (2008).

14 E. Yamamoto, G.H. Bokelman, N.G. Lewis, in: N.G. Lewis, M.G. Paice (Eds.), *Plant cell wall polymers, biogenesis and biodegradation*, American Chemical Society, Washington DC, Vol 399, 1989, pp. 68–88.

15 D. Klemm, B. Philipp, T. Heinze, et al., *Comprehensive Cellulose Chemistry,* Wiley-VCH, Weinheim, Vols. 1&2, 1998.

16 L. Fu, Y. Zhang, C. Li, Z. Wu, Q. Zhuo, et.al., *Skin tissue repair materials from bacterial cellulose by a multilayer fermentation method,* J. Mater. Chem. 22 (2012) 12349–12357.

17 G. Koch, in: H. Sixta (Ed.), *Handbook of Pulp*, Wiley-VHC, Weinheim, 2006, p. 24.

18 A. Potthast, T. Rosenau, P. Kosima, in: Klemm D. (Ed.), *Polysaccharides II. Advances in Polymer Science*, Springer, Berlin, Heidelberg, Vol. 205, 2006, p. 8.

19 A. Potthast, T. Rosenau, P. Kosima, in: Klemm D. (Ed.), *Polysaccharides II. Advances in Polymer Science*, Springer, Berlin, Heidelberg, Vol. 205, 2006, p. 3.

20 G. Koch, in: H. Sixta (Ed.), *Handbook of Pulp*, Wiley-VHC, Weinheim, 2006, pp. 24–28.

21 E. Gruber, *Pflanzenaufschluss (Grundlagen der Zellstoffherstellung) Kapitel 07: Cellulose,* http://www.gruberscript.net/07Cellulose.pdf. (Last update: 2012/09/12)

22 A. Rußler, *Substituentenverteilung an Cellulosexanthogenaten*, Dissertation, Universität Hamburg, 2005, pp. 2–3.

23 K. Karlsson, M. Carrillo Aguilera, L. Karlson et al., *Chain-Length Shortening of Methyl Ethyl Hydroxyethyl Cellulose: An Evaluation of the Material Properties and Effect on Foaming Ability*, J. Polym. Environ. 26 (2018) 4211–4220.

24 H. Sixta, *Handbook of Pulp*, Wiley-VHC, Weinheim, 2006.

25 G.A. Smook, *Handbook for Pulp & Paper Technologists*, 2nd ed., Angus Wilde Publications Inc., Vancouver, 1994, pp. 4–5.

26 D. Fengel, G. Wegener, *Wood: chemistry, ultrastructure, reactions*, De Gruyter, Berlin, 1989, pp. 73-77.

27 D. Fengel, G. Wegener, *Wood: chemistry, ultrastructure, reactions*, De Gruyter, Berlin, 1989, pp. 76–83.

28 D. Fengel, G. Wegener, *Wood: chemistry, ultrastructure, reactions*, De Gruyter, Berlin, 1989, pp. 83–100.

29 G.A. Jeffrey, W. Saenger, *Hydrogen Bonding in Biological Structures*, study ed., Springer, Berlin, Heidelberg, 1991, 1994, pp. 216–219.

30 A. Pinkert, K.N. Marsh, S. Pang, M.P. Staiger, *Ionic Liquids and Their Interaction with Cellulose,* Chem. Rev. 109 (2009) 6712–6728.

31 C.Y. Liang, R.H. Marchessault, *Infrared spectra of crystalline polysaccharides. II. Native cellulose in the region from 640-1700 cm*$^{-1}$, J. Polym. Sci. 39 (1959) 269–278.

32 J. Blackwell, F.J. Kolpak, K.H. Gardner, in: J.C. Arthur (Ed.), *Cellulose Chemistry and Technology,* American Chemical Society, Washington DC, Vol. 48, 1977, pp. 42–55.

33 M. Åkerholm, *Ultrastructural Aspects of Pulp Fibers as Studied by Dynamik FT-IR Spectroscopy,* Doctoral thesis, Royal Institute of Technology, 2003, pp. 21–22.

34 A. Rußler, *Substituentenverteilung an Cellulosexanthogenaten*, Dissertation, Universität Hamburg, 2005, pp. 5–7.

35 C.-F. Liu, R.-C. Sun, in: R.-C. Sun (Ed.), *Cereal Straw as a Resource for Sustainable Biomaterials and Biofuels: Chemistry, Extractives, Lignins, Hemicelluloses and Cellulose*, Elsevier, Amsterdam, 2010, pp. 138–143.

36 N. Le Moigne, *Swelling and dissolution mechanisms of cellulose fibres*, Doctoral thesis, École Nationale Supérieure des Mines de Paris, 2008, pp. 20–23.

37 D. Klemm, H.-P. Schmauder, T. Heinze, in: E. Vandamme, S. De Baets (Eds.), *Biopolymers: Biology, Chemistry, Biotechnology, Applications*, Wiley-VHC, Weinheim, Vol. 206: Polysaccharide II, 2002, pp. 277–319.

38 M. Ciudad-Mulero, V. Fernández-Ruiz, Mª C. Matallana-González, in: I. C. F. R. Ferreira, L. Barros (Eds.), *Advances in Food and Nutrition Research*, Elsevier, Amsterdam, Vol. 91, 2019, p. 87.

39 D. Fengel, G. Wegener, *Wood: chemistry, ultrastructure, reactions*, De Gruyter, Berlin, 1989, pp. 106–131.

40 M. Asif, L.B. Adams, in: J.M. Khatib (Ed.), *Sustainability of Construction Materials*, Woodhead Publishing, Cambridge, 2009, pp. 31–54.

41 M.H.B. Hayes, R. Mylotte, R.S. Swift, in: D.L. Sparks (Ed.), *Advances in Agronomy*. Elsevier, Amsterdam, Vol. 143, 2017, pp. 94–95.

42 J. Baeza, J. Freer, in: D.N.S. Hon, N. Shiraishi (Eds.), *Wood and Cellulosic Chemistry, Revised, and Expanded*, CRC Press, New York, 2000, pp. 300–304.

43 G. Koch, in: H. Sixta (Ed.), *Handbook of Pulp*, Wiley-VHC, Weinheim, 2006, pp. 28–41.

44 D. Fengel, G. Wegener, *Wood: chemistry, ultrastructure, reactions*, De Gruyter, Berlin, 1989, pp. 132–174.

45 D. Fengel, G. Wegener, *Wood: chemistry, ultrastructure, reactions*, De Gruyter, Berlin, 1989, pp. 182–221.

46 G.A. Smook, *Handbook for Pulp & Paper Technologists, 2nd ed.*, Angus Wilde Publications Inc., Vancouver, 1994, pp. 10–16.

47 D. Fengel, G. Wegener, *Wood: chemistry, ultrastructure, reactions*, De Gruyter, Berlin, 1989, pp. 13–16.

48 M. Fujita, H. Harada, in: D.N.S. Hon, N. Shiraishi (Eds.), *Wood and Cellulosic Chemistry, Revised, and Expanded*, CRC Press, New York, 2000, pp. 1–47.

49 G. Koch, in: H. Sixta (Ed.), *Handbook of Pulp*, Wiley-VHC, Weinheim, 2006, pp. 41–44.

50 G. Koch, in: H. Sixta (Ed.), *Handbook of Pulp*, Wiley-VHC, Weinheim, 2006, p. 41.

51 N. Le Moigne, *Swelling and dissolution mechanisms of cellulose fibres*, Doctoral thesis, École Nationale Supérieure des Mines de Paris, 2008, pp. 28–31.

52 H. Sixta, A. Potthast, A. W. Krotschek, in: H. Sixta (Ed.), *Handbook of Pulp*, Wiley-VHC, Weinheim, 2006, p. 110.

53 H. Sixta, A. Potthast, A. W. Krotschek, in: H. Sixta (Ed.), *Handbook of Pulp*, Wiley-VHC, Weinheim, 2006, pp. 109–510.

54 H.-P. Fink, H. Ebeling, W. Vorwerg, *Technologien der Cellulose- und Stärkeverarbeitung*, Chem. Ing. Tech. 81 (2009) 1757-1766.

55 P. Bajpai, *Pulp and Paper Industry: Energy Conservation*, Elsevier, Amsterdam, 2016, pp. 145–152.

56 A.P. Periyasamy, J. Militky, in: S. Muthu, M. Gardetti (Eds.), *Sustainability in the Textile and Apparel Industries*, Springer, Cham (CH), 2020, pp. 63-95.

57 R.P. Wollboldt, G. Zuckerstätter, H.K. Weber, P.T. Larsson, et al., *Accessibility, reactivity and supramolecular structure of E. globulus pulps with reduced xylan content*, Wood Sci. Technol. 44 (2010) 533–546.

58 D. Ibarra, V. Köpcke, M. Ek, *Exploring enzymatic treatments for the production of dissolving grade pulp from different wood and non-wood paper grade pulps*, Holzforschung 63 (2009) 721–730.

59 S. Saka, H.Matsumura, *2.3 Wood pulp manufacturing and quality characteristics*, Macromol. Symp., 208 (2004) 37–48.

60 T. Rosenau, A. Potthast, H. Sixta, P. Kosma, *The chemistry of side reactions and byproduct formation in the system NMMO/cellulose (Lyocell process),* Prog. Polym. Sci. 26 (2001) 1763–1837.

61 T. Rosenau, A. Potthast, W. Milacher, et al., *Isolation and identification of residual chromophores in cellulosic materials,* Polymer 45 (2004) 6437–6443.

62 P. White, in: C. Woodings (Ed.), *Regenerated Cellulose Fibres*, Woodhead Publishing Limited, Cambridge, 2001, pp. 62–87.

63 H. Sixta, in: H. Sixta (Ed.), *Handbook of Pulp*, Wiley-VHC, Weinheim, 2006, pp. 1009–1068.

64 A. Rußler, *Substituentenverteilung an Cellulosexanthogenaten*, Dissertation, Universität Hamburg, 2005, p. 4.

65 H. Sixta, A. Potthast, A. W. Krotschek, in: H. Sixta (Ed.), *Handbook of Pulp*, Wiley-VHC, Weinheim, 2006, p. 122.

66 H . Sixta, M. Iakovlev, L. Testova, A. Roselli et al., *Novel concepts of dissolving pulp production*, Cellulose 20 (2013) 1547–1561.

67 A. Shrotri, H. Kobayashi, A. Fukuoka, in: C. Song (Ed.), *Advances in Catalysis*, Academic Press, New York, Vol. 60, 2017, pp. 59-123.

68 M.T. Holtzapple, in: B. Caballero (Ed.), *Encyclopedia of Food Sciences and Nutrition, second ed.,* Academic Press, Amsterdam, 2003, pp. 3535-3542.

69 E.L. Springer, J.F. Harris, *Prehydrolysis of aspen wood with water and with dilute aqueous sulfuric acid,* Svensk. Papperstidn. 85 (1982) 152–154.

70 S.A. Rydholm, *Pulping Processes, orig. ed.*, Wiley & Sons Inc. New York, 1965 665.

71 E.L. Springer, *Hydrolysis of aspenwood xylan with aqueous solutions of hydrochloric acid*, Tappi. 49 (1966) 102–106.

72 Springer, E.L., L.L. Zoch, *Hydrolysis of xylan in different species of hardwoods*, Tappi, 51 (1968) 214–218.

73 A. Rodríguez, E. Espinosa, J. Domínguez-Robles, R. Sánchez, et. al., in: S. N. Kazi (Ed.) *Pulp and Paper Processing*, IntechOpen, London, 2018, pp. 33–54.

74 W. Wizani, et al., *Viscose production process,* PCT Pub. WO94/12719, 1994.

75 H. Sixta, A. Proberger, *Method for producing a type of pulp,* PCT Pub. WO2007/128026A1, 2007.

76 G. Schild, H. Sixta, L. Testova, *Multifunctional alkaline pulping, delignification and hemicellulose extraction*, Cellulose Chem. Technol. 44 (2010) 35–45.

77 B. Lönnberg, in: C. Woodings (Ed.), *Regenerated Cellulose Fibres*, Woodhead Publishing Limited, Cambridge, 2001, p. 33.

78 R. N. Miller, W. H. Swanson, *Chemistry of the Sulfite Process –Studies of the Acid Hydrolysis of Wood*, J. Ind. Eng. Chem. 17 (1925) 843–847.

79 M. G. Wolfinger, H. Sixta, *Modeling of the acid sulfite pulping process. – Problem definition and theoretical approach for a solution with the main focus on the recovery of cooking chemicals*, Lenzinger Ber. 83 (2004) 35–45.

80 H. Sixta, H.-U. Süss, A. Potthast, M. Schwanninger et al., in: H. Sixta (Ed.), *Handbook of Pulp*. Wiley-VHC, Weinheim, 2006, pp. 609–932.

81 H. Sixta, H.-U. Süss, A. Potthast, M. Schwanninger et al., in: H. Sixta (Ed.), *Handbook of Pulp*, Wiley-VHC, Weinheim, 2006, pp. 609–932.

81 G.A. Smook, *Handbook for Pulp & Paper Technologists*, *2nd ed.*, Angus Wilde Publications Inc., Vancouver, 1994, pp. 163–185.

83 M. Niaounakis, in: M. Niaounakis (Ed.), *Management of Marine Plastic Debris*, William Andrew Publishing, New York, 2017, pp. 1–55.

84 A. G. Wilkes, in: C. Woodings (Ed.), *Regenerated Cellulose Fibres*, Woodhead Publishing Limited, Cambridge, 2001, p. 37–61.

85 A. Rußler, *Substituentenverteilung an Cellulosexanthogenaten*, Dissertation, Universität Hamburg, 2005, pp. 10–27.

86 D. J. Mozdyniewicz, K. Nieminen, H. Sixta, *Alkaline steeping of dissolving pulp. Part I: Cellulose degradation kinetics*, Cellulose 20(3) (2013) 1437–1451.

87 R. Protz, G. Weidel, A. Lehmann, *Man-Made Cellulosic Fibers via the Viscose Process – New Opportunities by Cellulose Carbamate*, Lenzinger Ber. 94 (2018) 77–84.

88 K. Lauer, R. Jaks, L. Skark, *Zur Kenntnis der Xanthogenierung von Zellulose*; Kolloid-Z. 110 (1945) 26–34.

89 M. I. Tobler–Rohr, in: M. I. Tobler–Rohr (Ed.), *Handbook of Sustainable Textile Production*, Woodhead Publishing, New York, 2011, pp. 45–149.

90 K. Götze, *Chemiefasern nach dem Viskoseverfahren, dritte Auflage (überarbeitet)*, Springer, Berlin, Heidelberg, 2013.

91 D. Topgaard, O. Söderman, *Changes of cellulose fiber wall structure during drying investigated using NMR self-diffusion and relaxation experiment*s, Cellulose 9 (2002) 139–147.

92 S. Okubayashi, U.J. Griesser, T. Bechtold, *Water Accessibilities of Man-made Cellulosic Fibers – Effects of Fiber Characteristics*, Cellulose 12 (2005) 403–410.

93 G.V. Lisyakova, A.T. Serkov, K. I. Tsyganov, *Drying and conditioning viscose staple fibre*, Fibre Chem. 18 (1987) 444–449.

94 S. Mondal, P. Agarwala, P. Dutta et la., *Cellulosic fibre drying: fundamental understanding and process modeling*, in Proc. 21th International Drying Symposium (IDS 2018), (J. A. Cárcel, G. Clemente, J. V. García-Pérez, A. Mulet, C. Rosselló, eds.), Editorial Universitat Politècnica de València, Valencia (ES), 2018, pp. 627–634.

95 N. Allen, in: P. J. Vinken, G. W. Bruyn (Eds.), *Handbook of Clinical Neurology*, Elsevier/North Holland Biomedical Press, Amsterdam, 1979, pp. 361–389.

96 World Health Organization, *Carbon disulfide*, World Health Organization, 1979.

97 T. Hartikainen, J. Ruuskanen, P. J. Martikainen, *Carbon Disulfide and Hydrogen Sulfide Removal with a Peat Biofilter,* J. Air & Waste Manage. Assoc. 51 (2001) 387–392.

98 S. Zhang, C. Chen, C. Duan et al., Regenerated cellulose by the Lyocell process, a brief review of the process and properties, BioRes. 13(2) (2018) 4577–4592.

99 D. Loubinoux, S. Chaunis, *An Experimental Approach to Spinning New Cellulose Fibers with N-Methylmorpholine-Oxide as a Solvent*, Text. Res. J., 57(2) (1987) 61–65.

100 X. Colom, F. Carrillo, Crystallinity changes in lyocell and viscose-type fibres by caustic treatment, Eur. Polym. J. 38(11) (2002) 2225–2230.

101 W. Gindl-Altmutter, S. J. Eichhorn, M. Burghammer, J. Keckes, *Radial crystalline texture in a lyocell fibre revealed by synchrotron nanofocus wide-angle X-ray scattering*, Cellulose 21(1) (2014) 845–851.

102 T. Hongu, G. O. Phillips, *New Fibers 2nd Edition,* Woodhead Publishing, New York, 1997.

103 S. Böhmdorfer, T. Hosoya, T. Röder, et al., *A cautionary note on thermal runaway reactions in mixtures of 1-alkyl-3-methylimidazolium ionic liquids and N-methylmorpholine-N-oxide*, Cellulose 24 (2017) 1927–1932.

104 *Lenzing Group Sustainability Report 2007 – Non–Financial Statement,* Lenzing AG, Lenzing, 2017.

105 T. Rosenau, A. Potthast, I. Adorjan et al., *Cellulose solutions in N-methylmorpholine-N-oxide (NMMO) – degradation processes and stabilizers*, Cellulose 9 (2002) 283–291.

106 H.-P. Fink, P. Weigel, H. J. Purz, J. Ganster, *Structure formation of regenerated cellulose materials from NMMO-solutions*, Prog. Polym. Sci. 26 (9) (2001) 1473–1524.

107 U. Wachsmann, M. Diamantoglou, *Potential des NMMO-Verfahrens für Fasern und Membranen*, Das Papier, 51 (12) (1997), pp. 660–665.

108 S. Zhang, C. Chen, C. Duan et al., *Regenerated cellulose by the Lyocell process, a brief review of the process and properties*, BioRes. 13(2) (2018) 4577–4592.

109 A. P. Manian, T. Pham, T. Bechtold, in: A. R. Bunsell (Ed.), *In the Textile Institute Book Series, Handbook of Properties of Textile and Technical Fibres (Second Edition)*, Woodhead Publishing, New York, 2018, pp. 329–343.

110 O. Biganska, P. Navard, *Kinetics of precipitation of cellulose from cellulose−NMMO−water solutions*, Biomacromolecules 6 (2005) 1948–1953.

111 S. A. Mortimer, A. A. Peguy, *The influence of air-gap conditions on the structure formation of lyocell fibers*, J. Appl. Polym. Sci. 60 (1996) 1747–1756.

112 O. J. Rojas, *Cellulose Chemistry and Properties: Fibers, Nanocelluloses and Advanced Materials, Band 271 from Advances in Polymer Science*, Springer, Berlin, Heidelberg, 2016.

113 C. Guizani, K. Nieminen, M. Rissanen et al., *New insights into the air gap conditioning effects during the dry-jet wet spinning of an ionic liquid-cellulose solution*, Cellulose 27 (2020) 4931–4948.

114 E. Valkó, *Kolloidchemische Grundlagen der Textilveredelung*, Springer, Berlin, 1937.

115 R. Chavan, A. Patra, *Development and processing of lyocell*, Indian J. Fibre and Text. 29(4) (2004) 483.

116 A. J. Uddin, A. Yamamoto, Y. Gotoh et al., *Preparation and physical properties of regenerated cellulose fibres from sugarcane bagasse*, Text. Res. J. 80(17) (2010) 1846–1858.

117 K. Bredereck, F. Hermanutz, *Man-made cellulosics*, Rev. Prog. Color. 35 (2005) 59–75.

118 H.-G. Elias, *Macromolecules: Volume 1 · Structure and Properties / Volume 2 · Synthesis and Materials*, Springer, Berlin, Heidelberg, 2013, p. 480.

119 T. Kreze, S. Jeler, S. Strnad, *Correlation between structure characteristics and adsorption properties of regenerated cellulose fibers*, Mat. Res. Innovat. 5 (2002) 277–283.

120 T. Gries, D. Veit, B. Wulfhorst, *Textile Technology: An Introduction*, Carl Hanser Verlag, München, 2015, p. 346.

121 A. R. Bunsell, S. Joannès, A. Marcellan, in: A. R. Bunsell (Ed.), *Handbook of Properties of Textile and Technical Fibres (Second Edition)*, Woodhead Publishing, New York, 2018, pp. 21–55.

122 T. Luxbacher, *The Zeta Potential for Solid Surface Analysis – A practical guide to streaming potential measurement*, Anton Paar GmbH, Austria, 2014.

123 R. Zimmermann, W. Jenschke, H. Körber et al., *Bestimmung des Zeta-Potentials und der Grenzflächenleitfähigkeit durch Strömungspotential- und Strömungsstrommessungen*, Technisches Messen 67 (2000) 353– 360.

124 J. Liesiene, J. Kazlauske, *Functionalization of cellulose: Synthesis of water-soluble cationic cellulose derivatives*, Cellulose Chem. Technol. 47 (2013) 515–525.

125 E. Bialik, B. Stenqvist, Y. Fang et al., *Ionization of Cellobiose in Aqueous Alkali and the Mechanism of Cellulose Dissolution*, J. Phys. Chem. Lett. 7(24) (2016) 5044–5048.

126 T. G. M. Van De Ven, L. Godbout, *Cellulose: Fundamental Aspects*, BoD, Norderstedt, 2013, pp. 198–202.

127 P. Lian, R. C. Johnston, J. M. Parks et al., *Quantum Chemical Calculation of pK$_a$s of Environmentally Relevant Functional Groups: Carboxylic Acids, Amines and Thiols in Aqueous Solution*, J. Phys. Chem. A 122(17) (2018) 4366–4374.

128 C. J. Knill, J. F. Kennedy, *Degradation of cellulose under alkaline conditions*, Carbohydr. Polym. 51(3) (2003) 281–300.

129 H. Ohshima, K. Furusawa, *Electrical phenomena at interfaces: fundamentals, measurements, and applications – 2nd ed., rev. and expanded,* Dekker, New York, 1998.

130 F. Fairbrother, H. Mastin, *Studies in electro-endosmosis. Part 1*, J. Chemical Soc. 125 (1924) 2319-2330.

131 T. Luxbacher, in: R. M. Kozlowski, M. Mackiewicz-Talarczyk (Eds.), *Handbook of Natural Fibres: Volume 2: Processing and Applications*, Woodhead Publishing, New York, Vol. 2, 2020, pp. 323–392.

132 R. Zimmermann, U. Freudenberg, R. Schweiß et al., *Hydroxide and hydronium ion adsorption – A survey*, Curr. Opin. Colloid Interface Sci. 15 (2010) 196–202.

133 S. Temmel, W. Kern, T. Luxbacher, *Zeta Potential of Photochemically Modified Polymer Surfaces*, Progr Colloid Polym Sci 132 (2006) 54–61.

134 J. Schurz, *Was ist neu an den neuen Fasern der Gattung Lyocell?*, Lenzinger Berichte 74 (1994) 37–40.

135 J. Schurz, J. Lenz, *Investigations on the structure of regenerated cellulose fibers; Herrn Professor Janeschitz-Kriegl zum 70. Geburtstag mit den besten Wünschen gewidmet*, Macromol. Symp. 83(1) (1994) 273–289.

136 Reference Guide, *SurPASS™ 3, SurPASS™ 3 Eco,* Anton Paar GmbH, Austria, 2019.

137 N. G. Walter, *Single Molecule Tools, Part B: Super-Resolution, Particle Tracking, Multiparameter, and Force Based Methods*. Elsevier Science, Amsterdam, 2010, p. 604.

138 C. Lämmel, C. Heubner, T. Liebmann, M. Schneider, *Critical Impact of Chloride Containing Reference Electrodes on Electrochemical Measurements*, Electroanalysis, 29(12) (2017) 2752–2756.

139 A. V. Delgado, F. González-Caballero, R.J. Hunter, et al., *Measurement and interpretation of electrokinetic phenomena*, J. Colloid Interface Sci. 309 (2007) 194–224.

140 R. K. Schönfield, W. A. Taylor, *The hydrolysis of aluminium salt solutions*, J. Chem. Soc. 0 (1954) 4445-4448.

141 P. M. Mosur, Yu. M. Chernoberezhskii, A.V. Lorentsson, *Electrosurface Properties of Microcrystalline Cellulose Dispersions in Aqueous Solutions of Aluminum Chloride, Nitrate, and Sulfate*, Colloid Journal 70(4) (2008) 462–465.

142 J. W. Baty, W. Minter, S. Y. Lee, *The Role of Electrophilic Metal Ions AluminumIII and MagnesiumII in Paper Degradation and Deacidification,* The Book and Paper Group Annual 29 (2010) 113–120.

143 A. Rußler, M. Wieland, M. Bacher et al., *AKD-Modification of bacterial cellulose aerogels in supercritical CO2,* Cellulose 19 (2012) 1337–1349.

144 B. Schachtner, R. Smith, *Cellulosic fibres with hydrophobic properties*, PCT Pub. WO2013/067555A1, 2013.

145 B. Schachtner, G. Goldhalm, R. Smith, *Cellulosic fibre with hydrophobic properties and high softness and process for production thereof*, PCT Pub. WO2013/067556A1, 2013.